The Late Holocene tephra record of the central Mediterranean Sea: mapping occurrences and new potential isochrons for the 4.4-2.0 ka time interval

Insinga D.D.[1*], Petrosino P. [2], Alberico I.[1], de Lange G.J.[3], Lubritto C.[4], Molisso F.[1], Sacchi M.[1], Sulpizio R.[5], Wu, J.[3,6] & Lirer F.[1]

[1]Istituto di Scienze Marine (ISMAR)-CNR, Calata Porta di Massa, Interno Porto di Napoli, Napoli

[2]Dipartimento di Scienze della Terra dell'Ambiente e delle Risorse (DiSTAR), Università degli Studi "Federico II" di Napoli

[3]Department of Earth Sciences-Geochemistry, Utrecht University, The Netherlands

[4]Dipartimento di Scienze e Tecnologie Ambientali, Biologiche e Farmaceutiche, Università della Campania "Luigi Vanvitelli", Caserta

[5]Dipartimento di Scienze della Terra e Geoambientali, Università di Bari

[6]State Key Laboratory of Marine Geology, Tongji University, China

*: corresponding author

e-mail: donatelladomenica.insinga@cnr.it

Abstract

Five cores from the southern Tyrrhenian and Ionian seas have been studied for their tephra and cryptotephra content in the 4.4 - 2.0 ka time interval. The chronological framework for each core is obtained by Accelerator Mass Spectrometry ^{14}C dating, the occurrence of distinct marker tephra, and the stratigraphic correlation with adjacent records. Tephrochronology allows the correlation of the analyzed deposits with tephra markers associated with Somma-Vesuvius (79 AD), Ischia Island (Cretaio), Mt. Etna (FG, FL and FS) and Campi Flegrei (Astroni-Agnano Monte Spina) events. For the first time in the marine setting, a large single glass data set is provided for the Late-Holocene Etnean marker beds including the FS tephra (ca. 4.3 ka). Moreover, unknown deposits from Lipari (ca. 2.2-2.0 ka) and Vulcano (3.6-3.3 ka) have also been recognized at more distal sites than previously reported. These results contribute to improve the high-resolution tephrostratigraphic framework of the central Mediterranean Sea. They also provide new insights into the chemical composition and dispersal pattern of tephra that can be used as inter-archive tools for regional and "local" stratigraphic correlations and for addressing paleoclimate research.

Keywords: *tephra, cryptotephra, Italian volcanism, central Mediterranean, isochronous marker*

1. Introduction

The need for high-resolution, robust chronostratigraphic records, mainly for palaeoclimate research, has resulted in a significant development of tephra and cryptotephra studies during the last decade (e.g. Abbott *et al.,* 2018). This is particularly true for the central Mediterranean, a key area for tephrochronology due to the occurrence of active volcanoes during the Quaternary and the availability of long and continuous marine and continental archives (e.g. Keller *et al.*, 1978; Paterne *et al.*, 1988; 2008; Calanchi *et al.*, 1998; Siani *et al.*, 2004; Wulf *et al.*, 2004; Sulpizio *et al.*, 2010; Insinga *et al.*, 2014; Matthews *et al.*, 2015; Giaccio *et al.*, 2017). To date, in the marine setting , tephra and cryptotephra have been analyzed in ca. 129 sediment cores (198 in the whole Mediterranean) (Alberico *et al.*, 2017). As a result, more refined tephrostratigraphic frameworks for the Late Quaternary are now available from shelf to basin. They include mostly major tephra markers related to high-energy volcanic events (e.g. Wulf *et al.*, 2008; Zanchetta *et al.*, 2011; Bronk Ramsey *et al.*, 2015; Tomlinson *et al.*, 2015) and, to a lesser extent, deposits from moderately explosive eruptions (Sacchi *et al.*, 2009; Lirer *et al.*, 2013; Crocitti *et al.*, 2018; Di Donato *et al.*, 2019). These studies heavily rely on recent advancements in the methods and technology of sampling systems, that allow for the recovery of undisturbed sediment cores with the possibility of retrieving tephra and cryptotephra deposited in the last centuries even in the few centimeters of the sub-sea floor (e.g. Margaritelli *et al.*, 2016; Jalali *et al.*, 2018). Improved results in terms of tephra correlation also derived from high precision characterization of glass composition at proximal sites. A large database compiled in the last years for Somma-Vesuvius and Campi Flegrei volcanoes (Santacroce *et al.*, 2008; Smith *et al.*, 2011; Tomlinson *et al.*, 2012), for example, provided a significant contribution for the recognition of distal tephra and associated source vents. Conversely, for other eruptive centers, such as the Aeolian Islands and Mt. Etna, chemistry from single glass shards is available only for major markers (Albert *et al.*, 2012, 2013, 2017). As a result, a number of distal deposits, found both in the Tyrrhenian and Ionian seas and related to moderately explosive eruptions, are still uncorrelated (e.g. Paterne *et al.*, 1988; Di Donato *et al.*, 2018).

In this study we present a tephrostratigraphic framework for the 4.4 - 2.0 ka time interval of the central Mediterranean underpinned by the analysis of five marine cores. Our results are integrated with the Weather and Water Database (WDB)-Paleo which records paleoproxies metadata from the extensive marine core network (Alberico *et al.*, 2017). The main outcomes of this work include the detection of tephra with "local" correlation potential and the definition of robust isochrons for high-resolution stratigraphy.

2. Data set and analytical methods

2.1 Gravity cores

The tephra and cryptotephra analyzed in this work were sampled from cores located in the southern Tyrrhenian and Ionian Seas (Fig.1). They were collected between 1994 and 2012 in the frame of several research projects on board of the Research Vessel (R/V) Urania of the Italian Research Council (cores C14, C1, AP1.1, UM42BC) and the RV Pelagia (core CP10BC). Details are reported in Table 1.

Southern Tyrrhenian Sea

Gravity core C14 was recovered during the GMS98-01 cruise dedicated to the geological mapping of continental and marine areas (CARG project, 1997-2004). A 5.22 m long succession was retrieved from the western sector of Naples Bay at a depth of 186.5 m below sea level (bsl) and it is composed of silt deposits with volcaniclastic turbidites and interbedded primary tephra layers. The stratigraphic record sampled at C14 site spans the last ca. 9 ka (Petrosino et al., 2018).

Gravity core MSK-12 C1 (hereafter C1) was acquired during the MARISK_12 cruise along the eastern Tyrrhenian margin. The 4.50 m long record is located offshore Capo Vaticano at a depth of 604 m bsf and it is mostly composed of silt and interbedded primary tephra deposited during the last 17 ka (unpublished data).

Ionian Sea

Gravity core AP1.1 (hereafter AP1) was sampled in the northern Ionian during Sin-Sap 98 cruise. The 3.20 m long succession is located at 811 m bsl and characterized by silt deposits which include sapropel S1, S3 and S5 (D'Antonio *et al.*, 2016).

Box core UM42BC (hereafter UM42) was recovered in the western Ionian at a depth of 1375 m bsl during the oceanographic cruise Urania 18. It is 35.5 cm long and represented by hemipelagites with interbedded sapropel S1 (Freydier *et al.*, 2001).

Box core CP10BC (hereafter CP10) was collected during the CORTADO-2011 cruise at the Lybian-Tunisian slope. It is 35.5 cm long and characterized by marly ooze with the sapropel S1 as a distinct unit (Wu *et al.*, 2016, 2017).

2.2 Sampling and selection of the materials

Two visible tephra and four cryptotephra were sampled and analysed in this work (Tab.1). Where applicable (e.g. relatively thick deposits) or required for specific purposes (e.g. ultra high-resolution stratigraphic studies), a number of subsamples were taken from the same deposit. All

samples were labelled according to the identifying core code/name and the depth (cm) below the sea floor (bsf hereafter).

Sediment samples were disaggregated in distilled water and wet sieved at 63, 90, 125 and 250 μm in order to remove the fine-grained fraction. The sieved material was cleaned with an ultrasonic probe and dried at 60°C. A magnetic separator was used for scoria-rich samples. Subsequently, lithology was described using an optical microscope and fresh glass fragments were picked from selected samples for major-element characterization. As a criterion for the identification of cryptotephra, we selected the deposits where the juvenile fraction (mainly glass fragments) exceeded the 50% of the bulk sediment.

The visible tephra occur in cores C14 (89 - 74 cm bsf) and UM42 (7.4 - 6.7 cm bsf). The selected sample in core C14 (C14/89) includes the 89-87 cm bsf interval characterized by prevailing volcanic materials (Tab.1). Sample UM42/7 picked the 6.7-7.1 cm bsf interval where scoria fragments represent the 90% of the deposit (Tab.1 and Suppl. Fig.1).

In core CP10, the analyzed cryptotephra was recognized initially through the elemental composition of bulk sediments (Wu *et al.*, 2016, 2017). It is dispersed between 7 cm and 6.5 cm bsf (sample CP10/7) (Suppl. Fig.1).

In cores AP1 and C1, cryptotephra were identified by the inspection of washed sediments (>63 μm fraction) used for foraminifera analysis. The deposit investigated in core AP1 occurs between 13 cm and 12 cm bsf (sample AP1/13) whereas in core C1, two cryptotephra are dispersed between 56-52 cm bsf (sample C1/56) and along the 90-80 cm bsf interval. The latter was subsampled at 1-2 cm-step to observe possible changes in lithology and amount of the juvenile fraction. Four subsamples (C1/82, C1/85, C1/87 and C1/90) were selected for chemical characterization.

2.3 Major-element analysis

Juvenile fragments (pumice, scoria and glass shards) of samples selected from each deposit were mounted on epoxy resin and suitably polished for microprobe analyses performed on a SEM JEOL JSM 5310 (15 kV, ZAF Correction Routine) equipped with EDS at DiSTAR (University of Naples Federico II). Operating conditions were 15 kV primary beam voltage, 50–100 mA filament current, 50 s acquisition time with variable spot size. Correction for matrix effect was performed using INCA version 4.08 software that used the XPP correction routine, based on a Phi-Ro-Zeta approach. Primary calibration was performed using international mineral and glass standards. Details on the standards used are given in Morabito *et al.* (2014). Precision and accuracy were assessed using the rhyolitic Lipari obsidian ID3506 and basaltic Laki 1783 AD tephra (Kuehn et al., 2011) as secondary standards and the respective analytical values are reported in Supplementary Table 1 along with the analyses of individual glass fragments extracted from the studied deposits. Total oxide sums ≥93% were deemed acceptable considering that magmatic dissolved volatile components may reach >5% in evolved

trachytes and rhyolites (eg. Pearce *et al.*, 1999). The correlation of the analyzed tephra with proximal deposits or equivalents from different sites was based on the comparison of the new data with published SEM-EDS and WDS data where available. Criteria followed to infer primary origin of the studied deposits are described in Insinga *et al*. (2014).

2.3 ^{14}C AMS dating

Radiocarbon dating was performed on planktonic foraminifera collected from five samples in stratigraphic association with the analyzed tephra. Measurements were performed at the Poznań Radiocarbon Laboratory, at the J.G. van de Graaff laboratory (Utrecht University) and at INFN-Labec of Florence following procedures described in Goslar *et al.* (2004), van der Borg *et al.* (1997) and Lubritto *et al.* (2018), respectively. All the ^{14}C dates were converted into calendar ages using the Marine13 calibration curve (Reimer *et al.*, 2013) implemented in the program OxCal 4.3 (Bronk Ramsey, 2009) with no regional reservoir correction (i.e. $\Delta R=0$), which is valid for the modern Mediterranean (Siani *et al.*, 2000).

2.4 The WDB-Paleo database

The WDB-Paleo database includes data on about 6000 cores recovered from the Mediterranean Sea (Alberico *et al.*, 2017). It hosts metadata concerning paleoclimatic proxies, stratigraphic and chronological data (planktonic and benthic foraminifera, pollen, calcareous nanoplankton, magnetic susceptibility, oxygen stable isotope, AMS ^{14}C dating and tephra layers) published in ca. 200 scientific publications with associated reference information (authors, journal, books, years, title). Quantitative proxy data from all cores acquired in the frame of a number of Italian research projects were also integrated along with metadata on tephra from continental archives of central-southern Italy used in this work. A new entity hosting geochemical data has been implemented with data obtained here as shown in the logical model reported in Figure 2.

3. Results

3.1 Composition and sources of tephra

Lithological features of tephra (C14/89, UM42/7) and cryptotephra (C1/56, C1/80-90, AP1/13, CP10/7) are reported in Table 1. According to the TAS (total alkali-silica; Le Maitre, 2005) diagram and serial affinity (sodic to ultrapotassic), the analyzed samples are classified as basaltic trachyandesite, trachyphonolite and rhyolite, and from tephriphonolite to phonolite (Fig. 3a-b-c and Table 2). Tephra with Na-alkaline affinity occur in all cores except C14 (Fig.3c). Two geochemical populations characterize tephra C14/89 (phonolite + trachyphonolite), cryptotephra C1/85

(tephriphonolite-latite + mugearite), CP10/7 (rhyolite + mugearite) and AP1/13 (trachyphonolite + benmoreite) (Fig. 3). The overall chemical features of the analysed samples match well those of the Italian volcanic products and, in detail, with Mt. Etna, Aeolian Arc s.l., Somma-Vesuvius, Ischia Island and Campi Flegrei deposits (Fig. 3a and b, Tab.1). These correlations are consistent with the location of the core sites, downwind and in the proximity of source vents.

3.1.1 Mt. Etna related tephra

Deposits with Na-alkaline affinity (Fig.3c) can be classified as mugearites, benmoreites and trachytes in the TAS diagram (Fig. 3a-b). These compositions are typical of the intermediate-evolved products erupted by Mt. Etna volcano during the late Pleistocene-Holocene (Peccerillo, 2005) (Fig. 3a-b and Tab. 2). The analyzed tephra are mostly made of fine ash, which displays a crystalline groundmass of the juvenile materials with rare interstitial glass. Microlites are represented by clinopyroxene, plagioclase and opaques (Fig. 4a-b).

In core C1, the Etnean cryptotephra is dispersed in a relatively thick interval (ca. 10 cm) and it is characterized by a variable ratio between the content of juvenile fragments over the lithic and bioclastic fraction (Suppl. Fig. 1). No evidence of reworking has been observed. The content of the juvenile fraction in the selected samples ranges from 70% to 90% (C1/87 and C1/85) with respect to the biotic component in all the sieved fractions. Grayish pumice fragments occur with the ubiquitous dark scoria in sample C1/85. Glasses extracted from samples C1/90, C1/87 and C1/82, have a benmoreitic composition with some points falling also in the trachytic and tephriphonolitic field. In contrast, an almost homogenous mugearitic glass (a), along with minor tephriphonolitic glass (b) characterize sample C1/85 (Fig. 4b).

Tephra AP1/13 has a benmoreitic-mugearitic composition (a) and is associated with a minor trachyphonolitic glass (b).

Tephra UM42/7 is the only visible layer among the Etnean products. The deposit is well preserved and includes fresh juvenile fraction exceeding 85% over the whole lithic and biotic content. The juvenile materials are represented by aphyric and microlite bearing glass shards (Fig. 4c) and a minor component of porphyritic scoriae (Tab.1). A larger compositional variability characterizes this deposit, which has a mugearitic, benmoreitic and a trachytic composition. Trachytic points with SiO_2 concentration up to ca. 60 wt% are observed in aphyric glasses.

Tephra CP10/7 is characterized by a mugearitic population (a) with two glass fragments falling in the tephriphonolite field.

3.1.2 Aeolian Arc related tephra

Glass shards of cryptotephra CP10/7 appear light in color and characterized by a platy morphology at the optical observation. They have a rhyolitic composition (b) with a high-K calc-alkaline (HKCA) affinity typical of Lipari deposits erupted during the Late Pleistocene-Holocene (Fig. 3d and Tab.2). Cryptotephra C1/85b is a tephriphonolite with shoshonitic (SHO) affinity (Fig. 3d and Tab.2). Glasses are dark yellow and display a blocky morphology. Major element composition is quite homogenous: SiO_2 values range from 56.3 wt% to 57.6 wt%, FeO_{tot} from 5.8 wt% to 6.3 wt%, CaO from 3.4 wt% to 4.23 wt% and TiO_2 from 0.46 to 0.87 wt%. Volcanic products with such chemical composition have been erupted both by Stromboli and Vulcano during the Holocene (Fig. 3b).

3.1.3 Somma-Vesuvius, Ischia and Campi Flegrei related tephra

Tephra C14/89 is 15 cm-thick and formed by a medium-grained ash laying on a sharp erosive basal contact. Towards the top of the deposit, laminated structures containing biotite and lithics can be observed and the amount of the glass fraction over the lithic, crystal and bioclastic portion significantly decreases. Chemically, a phonolitic composition (a) coexists with a trachyphonolitic one (b) (Fig. 3a); both are very homogeneous in terms of major oxide concentration (Tab. 2). The phonolitic shards are characterized by SiO_2 average values of ca. 54.7 wt%, Al_2O_3 of ca. 20.5 wt%, Na_2O of ca. 4.7 wt%, K_2O of 9.7 wt% and FeO_{tot} of ca. 4.01 wt%. The trachyphonolitic glass shards display average SiO_2 values of ca. 62 wt%, CaO of ca. 1.5 wt% and Na_2O/K_2O=0.85. According to these chemical features, the phonolitic and trachyphonolitic populations of tephra C14/89 can be related to the highly and mildly silica-undersaturated potassic series of rocks (Fig. 3a-b) erupted by Somma-Vesuvius and Ischia volcanoes, respectively, during the Holocene (eg. Conticelli *et al.*, 2010).

Cryptotephra C1/56 is a fine ash made of mostly light grey micropumice. Leucite-bearing scoria and lithic fragments, obsidian, blocky glass shards and loose crystals also occur (Tab.1). Glass fragments have a phonolitic composition (Fig. 3a and Tab. 2) with SiO_2 values ranging from 54.8 wt% to 56.2 wt%, Al_2O_3 from 20 wt% to 22.74 wt%, Na_2O from 5 wt% to 7.37 wt% and CaO from 2.6 wt% to 5.6 wt%. Lithological features (e.g. occurrence of leucite) and composition suggest a correlation of C1/56 with Somma-Vesuvius deposits.

The minor trachyphonolitic component (b) occurring in cryptotephra AP1/13 is characterized by average SiO_2 value of 61.5 wt%, Al_2O_3 of ca. 18.46 wt% and K_2O/Na_2O= 1.77. These analyzed points display mildly silica-undersaturated potassic composition typical of Campi Flegrei products.

3.2 Age of tephra

AMS ^{14}C dates from cores C1, AP1, UM42 and CP10 are reported in Table 3. They are consistent with the stratigraphic position of the picked samples. Cryptotephra occurring in core C1 from 80 to

90 cm bsf is chronologically constrained by an age of 3625 ± 96 cal a BP obtained from a 2 cm-thick sample immediately below the deposit. Tephra UM42/7 occurs ~1 cm below sample DD01317 located at 5.65 (average) cm bsf and dated at 1797 ± 56 cal a BP. Since cosmogenic nuclides measurements indicate negligible loss of material from the core top (unpublished data), the mean sedimentation rate (SR) for the stratigraphic interval can be estimated in ca. 3 cm/ka. Extrapolating this SR down in the section for the very first few centimeters, we infer an age of ~2.2 cal ka for tephra UM42/7. The OxCal U_Sequence function (" ", 10) (Bronk Ramsey, 2008) was used to get a linear interpolated age for cryptotephra AP1/13 and CP10/7 constrained above and below by two radiocarbon ages (Tab. 3). This procedure yielded an age of 4237 ± 44 cal a BP for AP1/13 and of 2187 ± 37 cal a BP for UM42/7. The estimated SRs for the stratigraphic intervals containing the two cryptotephra are of ca. 3 cm/ka and 2.5 cm/ka, respectively.

4. Discussion

4.1 Proximal counterparts and marine equivalents

The tephrostratigraphic results and AMS ^{14}C ages are discussed for the studied deposits grouped according to their source vent. Most of tephra and cryptotephra are correlated with age dated volcanic events on land and/or with marine correlative layers in the central Mediterranean. Cross-correlations reveal the occurrence of two main marker tephra whereas other deposits have been recognized for the first time in the marine setting (Fig. 5).

4.1.2 Somma-Vesuvius, Ischia and Campi Flegrei

The phonolitic composition of C14/89a and C1/56 indicates the Somma-Vesuvius as the source volcano and the Pompeii 79 AD (Sigurdsson et al., 1985) as the source eruption (Figs. 3 and 6a). This event is widely recognized in areas adjacent to C14 core site in the Pozzuoli Bay (Sacchi *et al.*, 2014) and to C1 core site offshore Capo Vaticano (Cosentino *et al.*, 2017) (Fig.1). Lithology of tephra C14/89 in core C14 is distinctive of Pompeii deposits in the Naples and Pozzuoli bays. Sedimentological features include a significant thickness, an erosive bottom surface and parallel laminations, which suggest possible syneruptive reworking (Sacchi *et al.*, 2005; Insinga *et al.*, 2008). The correlation of cryptotephra C1/56 with Pompeii products is supported by its stratigraphic position in the C1 record above tephra unit C1/90-82 (ca. 3.6 cal ka BP; Tab.1). According to the FeO_{tot} vs CaO diagram (Fig. 6a), a continuous compositional variation trend from 79 AD grey to white pumice is observed in C1/56 whereas other distal equivalents display a single and/or twofold clusters. This includes C14/89a glass shards which display the grey pumice composition, and cryptotephra ND14_Q/79 from the southern Adriatic that is characterized by the white pumice chemistry (Fig. 1 and 6a).

The Ischia glass population of tephra C14/89b, matches well with Cretaio deposits (Orsi et al., 1992) (Fig. 3a), widely dispersed offshore the island (De Alteriis *et al.*, 2010). A number of radiocarbon datings from terrestrial and marine setting locate this event between 85 BC and 423 AD (Suppl. Tab.2). However, this large interval can be reasonably limited to the I century AD according to stratigraphic evidences from the marine settings i.e. the amalgamation of Cretaio and Pompeii deposits observed in the Pozzuoli Bay (Sacchi *et al.*, 2014) and in the southern Tyrrhenian (CET1 core site; Morabito et al., 2014) (Fig. 3a and 5).

The Campi Flegrei cryptotephra AP1/13b (4237 ± 44 cal a BP), can be correlated with the intense activity that occurred during the Late Holocene and produced mostly trachyphonolitic products. Their homogenous composition in terms of major elements makes a discrimination very difficult (Smith *et al.*, 2011). This is particularly true for the Agnano Mt. Spina and Astroni eruptions (AAMS group) reported between ca 4.4 and 4.6 cal ka BP and between ca 4.1 and 4.3 cal ka BP at proximal sites, respectively. (Smith *et al.*, 2011). In the marine setting, robust ages of 4166±114 cal a BP for Astroni tephra and 4422 ± 58 cal a BP for Agnano Mt.Spina tephra are provided by radiocarbon dating and age-depth modelling (Siani et al., 2004; Lirer et al., 2013) (Suppl. Tab.2). Distal products of AAMS group may occur either as multiple layers or amalgamated within one or more horizons (Siani *et al.*, 2004; Crocitti *et al.*, 2018). Although a discrimination criterion based on major element chemistry was proposed (Margaritelli *et al.*, 2016), the very low amount of glass shards found in the deposit hampers a robust statistic and hence we prefer to maintain a generic attribution of AP1/13b to AAMS group.

4.1.3 Lipari

Two HKCA rhyolitic glass shards occur in CP10/7b dated at 2187 ± 37 cal a BP. Distal cryptotephra with such a rhyolitic composition and a similar age have been found in cores KET80-03 (Paterne *et al.*, 1988) and TEA C6 (Di Donato *et al.*, 2019) in the southern Tyrrhenian and in the Gulf of Taranto, respectively (Fig. 5). In detail, a main Lipari rhyolitic population occurs at the top of KET core and it coexists with Eolian tephriphonolites (Fig. 3a) dated at ca. 1.7 ka based on sapropel chronology and isotope stratigraphy. In core TEA C6, cryptotephra C6/122 occurs immediately below the 79 AD tephra (C6/119) and it includes HKCA rhyolites with few reworked Pompei micropumice (Fig.3a) dated at 1.97 cal ka BP according to an age-depth model age constrained by tephrochronology and AMS ^{14}C dates. The proximal-distal correlation of this widespread deposit is hampered by the chronostratigraphy since no volcanic event is reported on the island at ca. 2 ka (e.g. Forni *et al.*, 2013)

4.1.4 Vulcano

According to the TAS and binary diagrams (Figs. 3b and 6b-c), we suggest a correlation of the tephriphonolitic (SHO) C1/85b with activity occurred at Vulcano Island. This is supported by the TiO_2 and Na_2O concentration of Vulcano deposits that display slightly different composition with respect to Stromboli shoshonitic products (Albert *et al.*, 2017). Tephra TIR2000-50 in the Marsili Basin (Di Roberto *et al.*, 2008; Albert *et al.*, 2012) is likely the marine equivalent of C1/85b (Figs. 5 and 6b-c). It occurs in core TIR2000-C01 stratigraphically below the Avellino-Pompeii (AP) interplinian deposits erupted at Somma-Vesuvius with age generally reported between 2.8 ka and 3.6 ka (Di Roberto *et al.*, 2008). The proximal-distal correlation of TIR2000-50 was discussed by Albert *et al.* (2012, 2017) but it remained unsolved. Although a perfect chemical match can be observed between C1/85b and TIR2000-50 with "Palizzi A" products emplaced at Vulcano at ca. 2 ka (Voltaggio *et al.*, 1995) (Figg.6b-c), this correlation is contrasting with the age of 3625 ± 96 cal a BP obtained just below our cryptotephra. Taking into account older activity on the island, a possibility of correlation with the Tufi di Grotte dei Rossi formation, constrained at ca. 4-5 ka (Lucchi *et al.*, 2008 and references therein), could have been hypothesized but the less evolved composition of these Vulcano deposits with respect to C1/85b excludes this possibility (Figs. 6b-c). In conclusion, C1/85b-TIR2000-50 tephra represents an unknown event, so far.

4.1.5 Mt. Etna

During the last 4 ka, intense volcanism at Etna produced a large number of tephra (Coltelli *et al.*, 1995). Among these are regional marker beds documented on land in the ca. 4.3 ka-2.0 ka time span and known as FS, FL, FG and FF (Coltelli *et al.*, 1998, 2000, 2005). Tephra FL and FG are reported at medial-distal sites in both marine and terrestrial settings whereas no records are documented for the other deposits outside the perivolcanic area, to date. The attribution of distal deposits to FL and FG relies mostly on their overall Etnean compositional affinity and age constraints. This is mostly due to the insufficiency of data available on these proximal deposits in terms of single glass shard chemistry. This paucity reflects the difficulties when comparing different datasets (generally bulk vs single glass analysis) to establish proximal-distal correlations and recognize the eruptive event (Insinga *et al.*, 2014). Moreover, the microlite-rich groundmass and the rare interstitial glass, which are typical features of these Etnean deposits (Coltelli *et al.*, 2000), make their chemical characterization a difficult task even at proximal sites. Our results are focused on more comprehensive single glass chemistry and dispersal in offshore areas and, in this context, they provide a new contribution towards a better understanding of these Late-Holocene Etnean deposits

The benmoreitic cryptotephra AP1/13a, represents the oldest Etnean deposit of this study. According to the age of 4237 ± 44 cal a BP and a SR value of 3 cm/ka for the analyzed stratigraphic interval, the studied deposit can be likely correlated with the FS subplinian eruption dated at 4360±92 cal a BP on land (Coltelli *et al.*, 2000, 2005).

The compositional field shown by subsamples of cryptotephra dispersed in the 90-80 cm interval bsf in core C1 (Fig. 3b and 6d) and the age result of 3625 ± 96 cal a BP immediately below, suggest a correlation of the deposit with the FL event, a complex phreatomagmatic eruption dated on land at 3361 ± 76 cal a BP (Coltelli *et al.*, 2000). At distal sites, the FL fall products display large chemical variability and may coexist with the AP deposits (Pepe et al., 2018; Di Donato *et al.*, 2019) (Figs.5 and 6d). At Lago di Pergusa, SE of Mt. Etna (Fig.1), where FL distal tephra was recognized for the first time and dated at ca. 3.3 cal ka BP (Sadori and Narcisi, 2001), single glass shards, instead, display a mugearitic composition close to that of C1/85a (Figs. 3b and 6d). Taking into account these observations along with the significant thickness in core C1, we infer that our cryptotephra may include the whole FL event. It was a long lasting eruption, likely older than ca. 3.3 cal ka BP, characterized by significant chemical variability and different dispersal of products. However, further comparisons with proximal deposits and datings are required to verify this working hypothesis.

According to the age of ca. 2.2 cal ka BP, tephra UM42/7 may be regarded as the distal counterpart of FG tephra dated between 380 BC and 120 AD and ascribed to the historical 122 BC Plinian event (Coltelli *et al.*, 1998) (Suppl. Tab.2). Eruptive products were dispersed mainly toward the SE and marine findings are reported in the Augusta Bay (De Martini et al., 2010; Smedile et al., 2011) and Malta Plateau (Micalleuf et al., 2016) (Fig. 8). Proximal and medial-distal glass data indicate a homogenous mugearitic composition of FG tephra (Fig. 3a) whereas at UM42 site the deposit reveals a wider chemical variability, which characterizes also other Etnean deposits at distal sites (Fig. 6d). To date, we suggest UM42/7 as the reference distal tephra of FG deposits for future correlations and further geochemical studies.

Taking into account the comparable age and the mugearitic composition (Figs.3b and 6d) along with the low SRs of cores CP10 and UM42 for the investigated time interval (2.5 cm/ka and 3 cm/ka, respectively), a correlation of cryptotephra CP10/7 with UM42/7 and therefore with FG tephra, is likely. This inference is also supported by dispersal direction and volume of 122 BC tephra, which is much higher than that of the almost coeval 44 BC tephra (Coltelli et al., 2000).

4.2 Tephra occurrences in the central Mediterranean Sea during the 4.2-2.0 ka time interval

Tephra correlation and dating results from this work have been included in the WdB-Paleo database in order to draw maps showing the occurrences of marker and minor tephra and newly discovered deposits in the central Mediterranean Sea (Figs. 7 and 8). Moreover, other major tephra, erupted during the investigated time interval but not occurring in our cores, have been also considered and mapped to provide a general overview of their distribution (Fig. 7). These are namely the Somma-Vesuvius related Avellino (3945 ± 10 cal a BP; Sevink *et al.*, 2011) and AP1-6 (ca. 2.8-3.6 cal ka BP;

Santacroce *et al.*, 2008 and references therein) tephra which represent important correlation tools given their significant areal distribution over southern Italy and surrounding seas (Fig. 7). If there is a general consensus on the proximal-distal correlation of the Avellino tephra across the basin, a large uncertainty still exists when attempting discrimination among the six AP events. This is likely due to their often overlapping chemical composition and insufficient chronological constraints, particularly concerning AP3-6 eruptive units, commonly reported younger than ca. 2.8 cal ka BP according to a single radiocarbon age (Suppl. Tab.2). However, recent results from the marine setting point to an ageing of the AP3-6 cluster as suggested by age-depth models (Sacchi et al., 2009; Lirer et al., 2013) (Suppl.Tab.2) and the finding of these deposits in association with FL tephra at distal sites (Pepe et al., 2018; Di Donato et al., 2019). According to these considerations, an age interval of ca. 3.6-3.4 cal ka BP for the AP eruptive sequence can be regarded as a working hypothesis to be further developed.

The maps obtained from the WdB-Paleo database provide a contribution to previous studies having implications on ash dispersal hazard related to both major and minor explosive events from Italian volcanoes (e.g. Sulpizio *et al.*, 2014; Crocitti *et al.*, 2018).

All the new occurrences of major tephra 79 AD, FL and AAMS group are well within their dispersal area (Fig. 7). The recent recovery of 79 AD deposits in the southern Adriatic, in particular, extends eastward their dispersal thus providing a key correlation marker for the three marine basins (Jalali et al., 2018). The recognition of FL tephra offshore Capo Vaticano represents its first finding in the southern Tyrrhenian. Accordingly, core C1 can be regarded so far as the most complete marine record where this long lasting eruption can be observed in its distal facies. Notwithstanding the scarce amount of glass shards, the recognition of AAMS group at the AP1 site is also of great interest, as it allows extending to the southeast (i.e. towards the northern Ionian) the dispersal of these products which are recorded in many Adriatic sequences.

The new finding in the Naples Bay of Cretaio tephra allows for the enlarging towards the east of the distribution of this deposit, which occurs significantly along the Campania margin, thus assuming a "local" stratigraphic relevance (Fig.8). The same ranking can be ascribed to the uncorrelated Vulcano tephra found between the Marsili Basin and Capo Vaticano offshore. The Lipari tephra has a striking regional significance, since it occurs in all the three marine areas surrounding the Italian peninsula and it is well age constrained in the Taranto Bay and at CP10 site. Finally, AP1, UM42 and CP10 represent the marine records where the Late Holocene FS and FG tephra occur. These site locations are in agreement with the ash dispersal toward E and SE (Coltelli *et al.*, 1998, 2005), respectively. In detail, cryptotephra AP1/13 is the first occurrence in the marine setting of FS deposits whereas UM42 and CP10 provides the more distal findings of FG tephra which can be definitely regarded as a regional stratigraphic marker.

4.3 Isochrons

The availability of continuous isocronous markers over wide areas of the central and western Mediterranean provides a means to verify the correlation of short and long-term climate oscillations between terrestrial and marine systems, enabling us to better understand the local-regional effects of climate change and the connections among different depositional environments (e.g. Margaritelli *et al.*, 2018). This integrated approach also represents a tool to match the possible interaction between climate changes and modifications of human societies and their adaptive strategies during the last millennia (e.g. Büntgen *et al.*, 2011; Holmgren *et al.*, 2016 and references therein). These are issues of great relevance for the study of the 4.4-2.0 ka time interval characterized by abrupt climatic changes (e.g. the 4.2 ka event; Bini *et al.*, 2019), increasing of human activities and, at the same time, recurrent explosive eruptions from different sources which produced widely dispersed tephra. Some of them, such as Agnano Monte Spina, Avellino and FL, have a relevant climatostratigraphic position in the Bronze Age (ca. 4.2 – 2.9 cal ka BP; Zanchetta *et al.*, 2018 and references therein) archives of the central Mediterranean. In this context, our work provides a number of isochronous stratigraphic horizons that have been traced according to our new results integrated with the WdB-Paleo database for the study area (Fig. 9).

The isochron corresponding to the 79 AD event crosses southern Italy and surrounding seas and, at some sites in the southern Tyrrhenian, it locally extends to the Cretaio tephra (I Century AD). This distinctive time horizon is immediately followed by the newly reported which covers the 2187±37 cal a BP - ca.1.97 k cal a BP time interval linking archives in the southern Tyrrhenian, Gulf of Taranto and south-western Ionian. It is targeted by the Lipari tephra at all sites and by a very well expressed FG tephra in the Ionian (Figs. 5-8-9). The ca. 3.6 -3.3 ka time interval can be traced in the whole area and targeted mostly by the AP deposits, locally also by FL (southern Tyrrhenian and Gulf of Taranto) and the undefined tephra from Vulcano (southern Tyrrhenian). Limitations in the use of this isochron may arise, however, from the chronological ambiguities previously described which can be solved only by further investigations at proximal sites and by critical revision of data at distal sites for the AP deposits. Similar considerations can be made for the 4422 ± 58 – 4237 ± 44 cal a BP time span targeted by AAMS group in the southern Tyrrhenian and Adriatic seas, in the Balkans and for the first time in the northern Ionian Sea where the Etnean FS tephra also occurs. The critical revision of distal tephra correlations, made according to the updated single glass database, might allow, in fact, discriminating the single event from Campi Flegrei within the AAMS group thus providing a narrower time interval for the study area.

5. Concluding remarks

The results presented in this work provide new insights into the chronology and distribution of tephra and cryptotephra in the central Mediterranean during the ca. 4.4-2.0 ka time interval. Analyzed

tephra comprised both markers associated to well-known, widespread Plinian events, and other deposits, characterized by narrower areal distribution or documented for the first time in the marine setting. These products have been characterized in detail, mapped and integrated with existing database to produce a high-resolution tephrostratigraphic framework for the basin. A further outcome of this work was the definition of five isochrons, which have the potential to correlate and synchronize paleoclimate archives. Further research developments to improve the stratigraphic framework presented in this study will likely require enhanced analysis of fine-grained cryptotephra and the solution of actual chronologic discrepancies for selected Late-Holocene volcanic events of the central Mediterranean region.

Acknowledgments

This work is dedicated to Urania R/V-CNR crews for their invaluable contribution to the marine research through the years. C. Corselli is acknowledged for many years of cooperation including Urania 1994 and 1998 cruises and UM42 and AP1.1 cores recovery. NWO/NIOZ is acknowledged for shiptime, NIOZ-technicians and Pelagia crew are thanked for the collaboration during Cortado-2011 cruise. R. de Gennaro is acknowledged for his assistance during the SEM-EDS acquisition and A. Filippidi for sorting out samples in Utrecht. Biagio Giaccio and an anonymous reviewer are acknowledged for their comments and suggestions that improved the quality of the manuscript.
M. Gore, D. Gahan and A. Fletcher helped D.D. Insinga to think of this "question of time" with the right mood. Financial support for Marisk12 cruise was provided by the Programma Operativo Nazionale (PON 2007-2013) funded by the Italian Ministry of University and Research – Project MONICA (grant PON01_01525). This research has been financially supported by the Project of Strategic Interest NextData PNR 2011-2013 (www.nextdataproject.it) and by the ERC-Consolidator TIMED project (REP-683237).

Supporting Information

Additional supporting information can be found in the online version of this article.

References

Abbott PM, Griggs AJ, Bourne AJ *et al.* 2018. Tracing marine cryptotephras in the North Atlantic during the last glacial period: Protocols for identification, characterisation and evaluating depositional controls. Marine Geology 401: 81–97.

Alberico I, Giliberti I, Insinga DD et al. 2017. Marine sediment cores database for the Mediterranean Basin: A tool for past climatic and environmental studies. Open Geosciences 9: 221-239

Albert PG, Tomlinson EL, Smith VC et al. 2012. Marine-continental tephra correlations: Volcanic glass geochemistry from the Marsili Basin and the Aeolian Islands, Southern Tyrrhenian Sea, Italy. Journal of Volcanology and Geothermal Research 229–230: 74–94.

Albert PG, Tomlinson EL, Lane CS et al. 2013. Late glacial explosive activity on Mount Etna: implications for proximal-distal tephra correlations and the synchronisation of Mediterranean archives. Journal of Volcanology and Geothermal Research 265: 9–26.

Albert PG, Tomlinson EL, Smith VC et al. 2017. Glass geochemistry of pyroclastic deposits from the Aeolian Islands in the last 50 ka: A proximal database for tephrochronology. Journal of Volcanology and Geothermal Research 336: 81–107.

Bini M, Zanchetta G, Perşoiu A et al. 2019. The 4.2 ka BP Event in the Mediterranean region: an overview. Climate of the Past 15: 555-577.

Bronk Ramsey C 2008. Deposition models for chronological records. Quaternary Science Reviews 27: 42–6.

Bronk Ramsey C 2009. Bayesian Analysis of Radiocarbon Dates. Radiocarbon 51: 337–360.

Bronk Ramsey C, Albert PG, Blockley SPE et al. 2015. Improved age estimates for key Late Quaternary European tephra horizons in the RESET lattice. Quaternary Science Reviews 118: 18–32.

Budillon F, Senatore MR, Insinga DD et al. 2012. Late Holocene sedimentary changes in shallow water settings: The case of the Sele River offshore in the Salerno Gulf (south-eastern Tyrrhenian Sea, Italy). Rendiconti Lincei 23: 25-43.

Büntgen U, Tegel W, Nicolussi K, et al. 2011. 2500 years of European Climate Variability and Human Susceptibility. Science 331: 578–82.

Çağatay MN, Wulf S, Sancar Ü et al. 2015. The tephra record from the Sea of Marmara for the last ca. 70 ka and its palaeoceanographic implications. Mar. Geol. 361: 96–110.

Calanchi N, Dinelli E, Lucchini F. et al. 1996. Chemostratigraphy of late Quaternary sediments from Lake Albano and central Adriatic Sea cores (PALICLAS Project). Memorie-Istituto Italiano di Idrobiologia. 55: 247–263.

Calanchi N, Cattaneo A, Dinelli E, et al. 1998. Tephra layers in Late Quaternary sediments of the central Adriatic Sea, Marine Geology 149: 191-209.

Calanchi N, Dinelli E, 2008. Tephrostratigraphy of the last 170 ka in sedimentary successions from the Adriatic Sea. Journal of Volcanology and Geothermal Research 177: 81–95.

Caron B, Sulpizio R, Zanchetta G, Siani G, Santacroce R, 2010. The Late Holocene to Pleistocene tephrostratigraphic record of Lake Ohrid (Albania). Comptes Rendus Geoscience 342: 453–466.

Cini Castagnoli G, Bonino G, Caprioglio F et al. 1990. The carbonate profile of two recent Ionian Sea cores: evidence that the sedimentation rate is constant over the last millennia. Geophys. Res. Lett. 17: 1937–1940.Coltelli M, Del Carlo P, Vezzoli L 1998. Discovery of a Plinian basaltic eruption of Roman age at Etna volcano, Italy. Geology 26: 1095–1098.

Coltelli M, Del Carlo P, Vezzoli L 1998. Discovery of a Plinian basaltic eruption of Roman age at Etna volcano, Italy. Geology 26: 1095-1098.

Coltelli M, Del Carlo P, Pompilio M et al. 2005. Explosive eruption of a picrite: The 3930 BP subplinian eruption of Etna volcano (Italy). Geophysical Research Letters 32, L23307

Coltelli M, Del Carlo P, Vezzoli L 2000. Stratigraphic constraints for explosive activity in the past 100 ka at Etna Volcano, Italy. International Journal of Earth Sciences 89: 665–677.

Conticelli S, Laurenzi MA, Giordano G et al. 2010. Leucite-bearing (kamafugitic/leucititic) and -free (lamproitic) ultrapotassic rocks and associated shoshonites from Italy: Constraints on petrogenesis and geodynamics. Journal of the Virtual Explorer 36: paper 20.

Cosentino C, Molisso F, Scopelliti G et al. 2017. Benthic foraminifera as indicators of relative sea-level fluctuations: Paleoenvironmental and paleoclimatic reconstruction of a Holocene marine succession (Calabria, south-eastern Tyrrhenian Sea). Quatenary International 439: 79–101.

Crocitti M, Sulpizio R, Insinga DD et al. 2018. On ash dispersal from moderately explosive volcanic eruptions: Examples from Holocene and Late Pleistocene eruptions of Italian volcanoes. Journal of Volcanology and Geothermal Research. https://doi.org/10.1016/j.jvolgeores.2018.07.009

D'Antonio M, Mariconte R, Arienzo I et al. 2016. Combined Sr-Nd isotopic and geochemical fingerprinting as a tool for identifying tephra layers: Application to deep-sea cores from Eastern Mediterranean Sea. Chemical Geology 443: 121–136.

De Alteriis G, Insinga D, Morabito S et al. 2010. Age of submarine debris avalanches and tephrostratigraphy offshore Ischia Island, Tyrrhenian Sea, Italy. Marine Geology 278: 1-18.

De Martini PM, Barbano MS, Smedile A, et al. 2010. A 4000 yrs long record of tsunami deposits along the coast of the Augusta Bay (eastern Sicily, Italy): paleoseismological implications. Marine Geology 276: 42–57.

Di Donato V, Insinga DD, Iorio M et al. 2019. The palaeoclimatic and palaeoceanographic history of the Gulf of Taranto (Mediterranean Sea) in the last 15 ky. Global and Planetary Change 172: 278–297.

Di Roberto A, Rosi M, Bertagnini A et al. 2008. Deep water gravity core from the Marsili Basin (Tyrrhenian Sea) records Pleistocenic-Holocenic explosive events and instability of the Aeolian Archipelago, (Italy). Journal of Volcanology and Geothermal Research 177: 133–144.

Forni F, Lucchi F, Peccerillo A, et al. 2013. Stratigraphic and geological evolution of the Lipari volcanic complex (central Aeolian archipelago). In: Lucchi, F., Peccerillo, A., Keller, J., Tranne, C.A., Rossi, P.L. (Eds.),The Aeolian Islands Volcanoes. Geological Society, London, Memoirs 37: 213–279.

Freydier R, Michard A, De Lange G et al. 2001. Nd isotopic compositions of Eastern Mediterranean sediments: Tracers of the Nile influence during sapropel S1 formation? Marine Geology 177: 45–62.

Geraga M, Mylona G, Tsaila-Monopoli ST et al. 2008. Northeastern Ionian Sea: Palaeoceanographic variability over the last 22 ka. Journal of Marine Systems 74: 623–638.

Giaccio B, Niespolo EM, Pereira A et al. 2017. First integrated tephrochronological record for the last ~190 kyr from the Fucino Quaternary lacustrine succession, central Italy. Quaternary Science Reviews 158: 211–234.

Goslar T, Czernik J, Goslar E 2004. Low-energy 14C AMS in Poznań Radiocarbon Laboratory, Poland. Nuclear Instruments and Methods in Physics Research, Section B: Beam Interactions with Materials and Atoms 223–224: 5–11.

Holmgren K, Gogou A, Izdebski A et al. 2016. Mediterranean Holocene climate, environment and human societies. Quaternary Science Reviews 136: 1-4.

Insinga D, Molisso F, Lubritto C et al. 2008. The proximal marine record of Somma Vesuvius volcanic activity in the Naples and Salerno bays, Eastern Tyrrhenian Sea, during the last 3 kyrs. Journal of Volcanology and Geothermal Research 177: 170–186.

Insinga DD, Tamburrino S, Lirer F et al. 2014. Tephrochronology of the astronomically-tuned KC01B deep-sea core, Ionian Sea: Insights into the explosive activity of the Central Mediterranean area during the last 200ka. Quaternary Science Reviews 85: 63-84.

Iorio M, Liddicoat J, Budillon F et al. 2009. Palaeomagnetic secular variation time constraint on Late Neogene geological events in slope sediment from the Eastern Tyrrhenian Sea. SEPM Spec. Publ. 92: 233–246.

Jalali B, Sicre MA, Klein V et al. 2018. Deltaic and coastal sediments as recorders of Mediterranean regional climate and human impact over the past three millennia. Paleoceanography and Paleoclimatology, DOI: 10.1029/2017PA003298.

Keller J, Ryan WBF, Ninkovich D 1978. Explosive volcanic activity in the Mediterranean over the past 200,000 yrs as recorded in deep-sea sediments. Geological Society of America Bulletin 89: 591-604.

Kuehn SC, Froese DG, Shane PAR et al. 2011. The INTAV intercomparison of electron-beammicroanalysis of glass by tephrochronology laboratories: results and recommendations. Quaternary International 246: 19–47.

Le Maitre RW 2005. Igneous rocks. A classification and glossary of terms. Recommendations of the International Union of Geological Sciences. Subcommission on the Systematics of Igneous Rocks. Cambridge: Cambridge University Press.

Lirer F, Sprovieri M, Ferraro L, et al. 2013. Integrated stratigraphy for the Late Quaternary in the eastern Tyrrhenian Sea. Quaternary International 292: 71-85

Lowe JJ, Blockley S, Trincardi F et al, 2007. Age modelling of late Quaternary marine sequences in the Adriatic: Towards improved precision and accuracy using volcanic event stratigraphy. Continental Shelf Research 27: 560-582.

Lubritto C, Ricci P, Germinario C et al. 2018. Radiocarbon dating of mortars: Contamination effects and sample characterisation. The case-study of Andalusian medieval castles (Jaén, Spain). Measurement: Journal of the International Measurement Confederation 118: 362–371.

Lucchi F, Tranne CA, De Astis G et al. 2008. Stratigraphy and significance of Brown Tuffs on the Aeolian Islands (southern Italy). Journal of Volcanology and Geothermal Research 177: 49-70.

Margaritelli G, Cisneros M, Cacho I, et al. 2018. Climatic variability over the last 3000 years in the central - western Mediterranean Sea (Menorca Basin) detected by planktonic foraminifera and stable isotope records. Global and Planetary Change 169: 179-187.

Margaritelli G, Vallefuoco M, Di Rita F et al. 2016. Marine response to climate changes during the last five millennia in the central Mediterranean Sea. Global and Planetary Change 142:53-72.

Matthews IP, Trincardi F, Lowe JJ et al. 2015. Developing a robust tephrochronological framework for Late Quaternary marine records in the Southern Adriatic Sea: New data from core station SA03-11. Quaternary Science Reviews 118: 84–104.

Micallef A, Georgiopoulou A, Mountjoy J, et al. 2016. Outer shelf seafloor geomorphology along a carbonate escarpment: the eastern Malta Plateau, Mediterranean Sea. Continental Shelf Research 131: 12-27.Morabito S, Petrosino P, Milia A et al. 2014. A multidisciplinary approach for reconstructing the stratigraphic framework of the last 40ka in a bathyal area of the eastern Tyrrhenian Sea. Global and Planetary Change 123: 121–138.

Morabito S, Petrosino P, Milia A et al. 2014. A multidisciplinary approach for reconstructing the stratigraphic framework of the last 40 ka in a bathyal area of the eastern Tyrrhenian Sea. Global and Planetary Change 123; 121-138.

Munno R, Petrosino P 2004. New constraints on the occurrence of Y-3 upper Pleistocene tephra marker layer in the Tyrrhenian Sea. Il Quaternario 17 (1): 11-20.

Munno R, Petrosino P 2007. The late Quaternary tephrostratigraphical record of the San Gregorio Magno basin (southern Italy). Journal of Quaternary Science 22: 247–266.

Orsi G, Gallo G, Heiken G et al 1992. A comprehensive study of pumice formation and dispersal: the Cretaio Tephra of Ischia (Italy). Journal of Volcanology and Geothermal Research 53: 329-354.

Paterne M, Guichard F, Duplessy JC et al. 2008. A 90,000-200,000 yrs marine tephra record of Italian volcanic activity in the Central Mediterranean Sea. Journal of Volcanology and Geothermal Research 177: 187–196.

Paterne M, Guichard F, Labeyrie J 1988. Explosive activity of the South Italian volcanoes during the past 80,000 years as determined by marine tephrochronology. Journal of Volcanology and Geothermal Research 34: 153–172.

Pearce NJG, Westgate JA, Perkins WT et al. 1999. The application of laser ablation ICP-MS to the analysis of volcanic glass shards from tephra deposits: Bulk glass and single shard analysis. Global and Planetary Change 21: 151–171.

Peccerillo A 2005. Petrogenesis and Geodynamics in Italy. Plio-Quaternary Magmatism in Italy Petrology, Geochemistry, Geodynamics. Springer, Heidelberg.

Pepe F, Di Donato V, Insinga D et al. 2018. Seismic stratigraphy of upper Quaternary shallow-water contourite drifts in the Gulf of Taranto (Ionian Sea, southern Italy), Marine Geology 397: 79-92.

Petrosino P, Insinga DD, Molisso F et al. 2018. Tephra markers for the timing of morphotectonic phases in the Campi Flegrei caldera. Crossing New Frontiers INTAV International Field Conference on Tephrochronology “Tephra Hunt in Transylvania” Moieciu de Sus, Romania. 24 June - 1 July 2018

Reimer PJ, Bard E, Bayliss A et al. 2013. IntCal13 and Marine13 Radiocarbon Age Calibration Curves 0–50,000 Years cal BP. Radiocarbon 55: 1869–1887. Sacchi M, Insinga D, Milia A et al. 2005. Stratigraphic signature of the Vesuvius 79 AD event off the Sarno prodelta system, Naples Bay. Marine Geology 222–223:443-469.

Sacchi M, Insinga D, Milia A, et al. 2005. Stratigraphic signature of the Vesuvius 79 AD event off the Sarno prodelta system, Naples Bay. Marine Geology 222-223: 443-469.

Sacchi M, Molisso F, Violante C et al. 2009. Insights into flood-dominated fan-deltas: Very high-resolution seismic examples off the Amalfi cliffed coasts, eastern Tyrrhenian Sea. In: Geohazard in Rocky Coastal Areas. The Geological Society, London, Special Publications, 322, 33–71.

Sacchi M, Pepe F, Corradino M et al. 2014. The Neapolitan Yellow Tuff caldera offshore the Campi Flegrei: Stratal architecture and kinematic reconstruction during the last 15 ky. Marine Geology 354: 15-33.

Sadori L, Narcisi B, 2001. The postglacial record of environmental history from Lago di Pergusa, Sicily. Holocene 11 (6): 655–670.

Sadori L, Ortu E, Peyron O et al. 2013. The last 7 millennia of vegetation and climate changes at Lago di Pergusa (central Sicily, Italy). Climate of the Past 9: 1969–1984.

Santacroce R, Sulpizio R, Zanchetta G et al 2008. Age and whole rocks-glass composition of proximal pyroclastics from the major explosive eruptions of Vesuvius: a review as a tool for distal tephrostratigraphy. Journal of Volcanology and Geothermal Research 177: 1-18.

Sevink J, van Bergen MJ, van der Plicht et al. 2011. Robust date for the Bronze Age Avellino eruption (Somma-Vesuvius): 3945 ± 10 cal BP (1995 ± 10 cal BC). Quaternary Science Reviews 30: 1035–1046.

Siani G, Paterne M, Arnold M et al. 2000. Radiocarbon Reservo Ir Ages in the Mediterranean Sea and Black Sea. Radiocarbon 42: 271–280.

Siani G, Sulpizio R, Paterne M et al. 2004. Tephrostratigraphy study for the last 18,00014C years in a deep-sea sediment sequence for the South Adriatic. Quaternary Science Reviews 23: 2485–2500.

Sigurdsson H, Carey S, Cornell W et al. 1985. The eruption of Vesuvius in A.D. 79. Natl. Geogr. Res. 1, 332–387.

Smedile A, De Martini PM, Pantosti D et al. 2011. Possible tsunami signatures from an integrated study in the Augusta Bay offshore (eastern Sicily-Italy). Marine Geology 281: 1–13.

Smith VC, Isaia R, Pearce NJG 2011. Tephrostratigraphy and glass compositions of post-15 kyr Campi Flegrei eruptions: Implications for eruption history and chronostratigraphic markers. Quaternary Science Reviews 30: 3638–3660.

Sulpizio R, Bonasia R, Dellino P, et al. 2008. Discriminating the long distance dispersal of fine ash from sustained columns or near ground ash clouds: The example of the Pomici di Avellino eruption (Somma-Vesuvius, Italy). Journal of Volcanology and Geothermal Research 177: 263–276.

Sulpizio R, Van Welden A, Caron B et al. 2010. The Holocene tephrostratigraphic record of Lake Shkodra (Albania and Montenegro). Journal of Quaternary Science 25: 633–650.

Sulpizio R, Zanchetta G, Caron B et al. 2014. Volcanic ash hazard in the Central Mediterranean assessed from geological data. Bulletin of Volcanology 76: 866-873.

Tomlinson EL, Arienzo I, Civetta L et al. 2012. Geochemistry of the Phlegraean Fields (Italy) proximal sources for major Mediterranean tephras: Implications for the dispersal of Plinian and co-ignimbritic components of explosive eruptions. Geochimica et Cosmochimica Acta 93:102–128.

Tomlinson EL, Smith VC, Albert PG et al. 2015. The major and trace element glass compositions of the productive Mediterranean volcanic sources: tools for correlating distal tephra layers in and around Europe. Quatenary Science Reviews 118: 48–66.

Van Der Borg K, Alderliesten C, De Jong AFM et al. 1997. Precision and mass fractionation in14C analysis with AMS. Nuclear Instruments and Methods in Physics Research, Section B: Beam Interactions with Materials and Atoms 123: 97–101.

Vogel H, Zanchetta G, Sulpizio R, et al. 2010. A tephrostratigraphic record for the last glacial-interglacial cycle from Lake Ohrid, Albania and Macedonia. Journal of Quaternary Science 25: 320–338.

Voltaggio M, Branca M, Tuccimei P et al 1995. Leaching procedure used in dating young potassic volcanic rocks by the 226Ra/230Th method. Earth and Planetary Science Letters 136: 123–131.

Wu J, Böning P, Pahnke K et al. 2016. Unraveling North-African riverine and eolian contributions to central Mediterranean sediments during Holocene sapropel S1 formation. Quaternary Science Reviews 152: 31–48.

Wu J, Liu Z, Stuut JBW et al. 2017. North-African paleodrainage discharges to the central Mediterranean during the last 18,000 years: A multiproxy characterization. Quaternary Science Reviews 163: 95–113.

Wulf S, Kraml M, Brauer A et al. 2004. Tephrochronology of the 100ka lacustrine sediment record of Lago Grande di Monticchio (southern Italy). Quaternary International 122: 7–30.

Wulf S, Kraml M, Keller J 2008. Towards a detailed distal tephrostratigraphy in the central Mediterranean: the last 20,000 yrs record of Lago Grande di Monticchio. Journal of Volcanology and Geothermal Research 177: 118-132.

Zanchetta G, Sulpizio R, Roberts CN et al. 2011. Tephrostratigraphy, chronology and climatic events of the Mediterranean basin during the Holocene: an overview. The Holocene 21 (1): 33-52.

Zanchetta G, Bini M, Di Vito MA et al. 2018. Tephrostratigraphy of paleoclimatic archives in central Mediterranean during the Bronze Age. Quaternary International 499: 186-194.

Core	Location		Depth below sea level (m)	Length (m)	Age control along the record	Tephra-Event (Source)	*Type* /Lithology	Composition	Age on proximal	Age in marine setting
C14	14°11'30" E	40°44'47"N	186.5	5.22	stratigraphic relation with other cores	C14/89-Pompei+Cretaio (SV+I)	*Visible tephra* /Light and light grey micropumice, dark scoria, lithics (some leucite bearing), loose crystals of feldspar and clinopyroxene.	Phonolite (population a) + Trachyphonolite (population b)	79 AD/I Century AD [(1)]	3 ± 42 AD for Cretaio [(2)]
C1	15°48.236' E	38°44.573'N	604	4.5	^{14}C and stratigraphic relation with other cores	C1/56-Pompei (SV)	*Cryptotephra* /Light and light grey vesiculated micropumice, leucite bearing lithics, loose crystals of feldspar and biotite	Phonolite	79 AD	-
						C1/82-FL (Et)	*Cryptotephra* /Dark to iron-grey porphyritic scoriaceous fragments, loose crystals and reddish lava lithic fragments	Benmoreite	3361±76 cal a BP (FL) [(3)]	
						C1/85-?(Vulc)+FL (Et)	*Cryptotephra* /Dark dense scoria and greysh pumice. Dark honey glass shards with blocky morphology also occur. Loose crystals of olivine, pyroxene and brown mica.	Mugearite (population a) + Tephriphonolite (SHO) (population b)		
						C1/87-FL (Et)	*Cryptotephra* /Dark porphyritic scoria and greysh pumice. Loose crystals of feldspar and clinopyroxene	Benmoreite-Trachyte		
						C1/90-FL (Et)	*Cryptotephra* /Dark grey porphyritic scoria	Benmoreite		3625 ± 96 cal a BP *(this study)*
SAPGCAP1.1	19°06.78'E	39°12.99'N	810	3.2	^{14}C datings, sedimentation rates	AP1/13*-FS+AAMS (Et+CF)	*Cryptotephra* /Dark grey dense scoria and rare pale gey pumice.	Benmoreite (population a) + Trachyphonolite (population b)	4.36 ± 0.092 cal ka BP[(3)]/4.6-4.1 cal ka BP [(4)]	4420 ± 60 cal a BP [(5);] 4237 ± 44 cal a BP *(this study)*
UM42BC	17°51.75'E	34°57.23'N	1375	0.355	^{14}C datings, sedimentation rates	UM42/7*-FG (Et)	*Visible tephra* /Brown to yellowish vesiculated glass fragments with feldspar crystals and minor honey dense aphyric glass fragments. Dark brown and grayish brown porphyritic scoria fragments, reddish lithics and loose crystals.	Mugearite to Benmoreite	380 BC-120 AD (122 BC historical age)[(6)]	~2.2 cal ka BP *(this study)*
CP10BC	16°34.00'E	34°32.70'N	1501	0.355	^{14}C datings, sedimentation rates	CP10BC/7*-FG+? (Et+L)	*Cryptotephra* /Dark scoria, altered micropumice and few platy glass shards. Loose crystals of feldspar and brown mica	Mugearite-Tephriphonolite (population a) + HKCA Rhyolite (population b)	380 BC-120 AD (122 BC historical age)[(6)]	1.97 cal ka BP for Lipari rhyolites [(7)] 2187 ± 37 cal a BP *(this study)*

Table 1. Summary of core and tephra data presented in this work including source volcano and event. Et: Etna, CF: Campi Flegrei, SV: Somma-Vesuvius, L:

Lipari, Vulc: Vulcano; (1) age for Cretaio from Orsi *et al.* (1992); (2) De Alteriis *et al.* (2010); (3) Coltelli *et al.* (2000); (4) Smith *et al.* (2011); (5) Lirer *et al.* (2013); (6) Coltelli *et al.* (1998); (7) Di Donato *et al.* (2019). *Original sample code on board: AP1/13=GG0128, UM42/7=DD1320; CP10/7=CP10BC#14.

Core	CP10BC									AP1.1								C14					
Sample	CP10/7a							CP10/7b		AP1/13a					AP1/13b			C14/89a			C14/89b		
cm bsf	6.5-7									12-13								88-89					
SiO_2	53,91	54,04	52,50	52,20	52,71	51,57	51,92	75,29	75,91	54,90	54,81	54,09	54,25	53,31	61,76	61,29	61,48	54,95	54,50	54,65	62,12	62,14	61,93
TiO_2	1,78	2,06	1,76	1,65	1,68	1,76	1,98	0,00	0,00	2,42	1,75	1,88	1,84	2,15	0,65	0,49	0,35	0,40	0,59	0,55	0,68	0,71	0,66
Al_2O_3	16,08	15,81	16,02	16,67	18,25	17,00	17,26	13,67	13,14	16,16	19,34	16,68	16,72	15,37	18,52	18,30	18,57	20,64	20,42	20,62	18,49	18,53	18,38
FeO	8,79	8,24	8,84	8,71	8,30	9,50	9,04	1,41	1,57	9,04	6,37	8,00	8,74	10,13	3,12	3,70	2,85	3,87	4,19	3,95	3,13	2,87	3,24
MnO	0,27	0,39	0,22	0,33	0,04	0,27	0,12	0,00	0,00	2,12	1,71	2,90	2,70	0,02	0,64	0,57	0,34	0,10	0,37	0,25	0,17	0,09	0,00
MgO	2,42	2,56	3,31	2,96	2,58	3,49	3,59	0,00	0,21	0,00	0,21	0,28	0,00	3,36	0,41	0,17	0,32	0,28	0,16	0,24	0,37	0,40	0,51
CaO	3,52	4,07	6,48	6,84	7,01	7,75	7,29	0,76	0,92	4,69	6,18	5,53	5,65	4,93	1,64	1,64	2,03	3,90	4,36	4,23	1,45	1,48	1,52
Na_2O	5,34	5,12	4,67	5,18	4,70	4,81	4,71	2,87	2,41	6,10	6,15	5,08	4,59	4,50	4,61	4,19	5,34	4,68	4,71	4,88	5,90	6,05	6,09
K_2O	5,78	5,53	4,31	3,23	3,49	2,39	2,44	5,21	4,89	3,44	2,27	4,01	4,09	4,57	7,95	8,85	8,17	9,75	9,57	9,73	7,07	7,14	6,90
P_2O_5	1,27	1,21	1,08	1,60	0,70	0,87	0,97	0,19	0,00	1,02	1,11	1,18	1,15	1,46	0,11	0,18	0,00	0,00	0,13	0,16	0,06	0,20	0,10
Cl	0,42	0,48	0,41	0,31	0,28	0,30	0,34	0,30	0,47	0,11	0,12	0,36	0,28	0,21	0,60	0,61	0,55	0,87	0,82	0,72	0,51	0,40	0,44
Original Total	97,59	99,83	97,69	98,23	96,40	97,38	96,17	95,88	95,31	97,38	100,87	97,28	97,49	100,22	96,11	94,79	98,07	98.49	97.43	98,12	97,47	96,78	98,77
Core	UM42BC																						
Sample	UM42/7																						
cm bsf	6.7-7.1																						
SiO_2	59,58	52,87	55,86	55,11	51,72	51,87	52,74	54,47	52,16	53,75	58,59	57,10	51,61	51,97	51,71	57,07	52,17	51,85	54,95	52,10	52,09	51,53	53,81
TiO_2	1,26	1,17	1,40	1,81	1,77	1,65	1,93	2,02	1,94	2,44	1,40	1,49	1,81	1,89	1,50	1,56	1,84	1,74	1,61	1,63	1,69	1,86	1,64
Al_2O_3	17,50	17,04	17,98	17,20	16,42	17,40	17,16	17,62	17,01	16,18	18,18	18,17	17,58	17,18	17,22	18,43	17,44	16,60	17,78	17,34	17,26	17,35	17,18
FeO	5,25	9,24	6,40	7,35	9,63	8,89	8,52	8,19	8,66	8,10	5,22	5,95	8,49	8,46	8,84	6,35	8,52	9,77	7,05	8,71	8,83	9,05	8,24
MnO	0,10	0,15	0,41	0,13	0,00	0,35	0,00	0,03	0,41	0,10	0,21	0,37	0,27	0,04	0,25	0,23	0,08	0,11	0,17	0,13	0,25	0,23	0,27
MgO	1,38	3,56	2,41	2,74	3,87	3,53	3,49	2,98	3,37	3,10	1,56	2,37	3,46	3,32	3,45	1,95	3,55	3,47	2,63	3,43	3,45	3,76	2,94
CaO	2,64	7,43	4,92	5,56	7,51	7,68	7,21	5,80	7,23	5,81	2,72	4,96	7,11	7,57	7,58	4,02	7,39	6,80	5,32	7,42	7,33	7,27	5,94
Na_2O	6,70	4,45	5,84	5,64	5,13	5,12	5,29	4,75	5,08	5,45	6,98	5,17	4,79	5,12	4,85	5,34	4,82	4,76	5,54	4,68	5,13	4,80	5,40
K_2O	4,58	2,52	3,56	3,32	2,52	2,47	2,32	3,18	2,59	3,31	4,25	3,11	2,42	2,44	2,42	3,58	2,47	2,93	3,17	2,49	2,42	2,50	2,97
P_2O_5	0,50	1,14	0,87	0,67	0,95	0,77	0,93	0,64	1,21	1,34	0,47	0,64	1,24	1,02	1,02	0,71	1,14	1,18	0,80	1,09	0,95	0,98	0,77
Cl	0,52	0,43	0,34	0,48	0,48	0,25	0,40	0,31	0,34	0,41	0,40	0,36	0,31	0,30	0,30	0,37	0,33	0,43	0,38	0,36	0,31	0,39	0,27
Original Total	98,59	95,71	97,35	98,48	96,94	98,46	97,94	97,80	99,18	98,13	94,98	96,82	97,05	98,37	98,16	98,47	97,94	98,67	97,62	97,41	97,1	97,95	98,22
Core	UM42BC																						
Sample	UM42/7																						
cm bsf	6.7-7.1																						
SiO_2	52,21	52,27	52,13	53,55	52,02	51,93	54,02	51,90	52,36	59,66	52,08	59,63	54,70	59,22	58,32	53,98	55,85	51,13	51,34	53,13	51,89		
TiO_2	1,94	1,98	1,89	1,69	1,72	1,99	1,74	2,17	1,84	1,10	1,96	1,05	1,88	1,15	1,40	1,56	1,34	1,78	1,71	1,61	1,96		
Al_2O_3	16,49	16,73	16,96	17,00	17,00	17,25	18,15	17,18	17,11	18,79	17,06	18,66	17,51	18,88	18,04	17,38	18,02	17,41	17,26	17,23	16,49		
FeO	9,05	9,16	8,93	8,35	9,10	8,13	8,89	8,65	8,25	4,97	8,69	4,99	7,33	5,39	5,92	8,01	6,53	9,32	9,08	8,12	9,05		
MnO	0,17	0,17	0,13	0,09	0,05	0,24	0,17	0,15	0,25	0,14	0,18	0,21	0,25	0,15	0,16	0,17	0,23	0,28	0,00	0,21	0,19		
MgO	3,72	3,63	3,59	3,00	3,66	3,46	1,97	3,67	3,55	1,31	3,64	1,39	2,99	1,38	1,47	2,81	2,23	3,81	3,47	2,99	3,17		
CaO	7,24	7,37	7,14	6,03	7,40	7,86	6,77	7,22	7,44	3,08	7,44	2,98	5,71	3,24	2,92	5,80	4,53	7,65	7,16	6,19	7,08		
Na_2O	4,74	4,28	5,17	5,38	4,75	5,18	4,05	5,03	5,09	5,51	5,02	5,74	4,98	5,49	6,10	5,20	6,03	4,38	5,42	5,74	5,58		
K_2O	2,89	2,58	2,47	3,21	2,49	2,40	2,28	2,54	2,46	4,06	2,44	4,12	3,09	4,00	4,41	3,17	3,45	2,40	2,57	2,95	2,78		
P_2O_5	0,89	0,99	0,80	0,98	0,93	0,84	0,87	0,95	0,93	0,22	0,94	0,36	0,93	0,27	0,54	0,86	0,56	0,95	1,05	1,10	0,93		
Cl	0,31	0,35	0,35	0,33	0,25	0,28	0,25	0,26	0,25	0,51	0,32	0,41	0,35	0,45	0,41	0,30	0,34	0,32	0,35	0,27	0,36		
Original Total	96,67	97,82	98,86	98	97,75	98,35	96,03	97,28	95,99	97,65	98,31	97,2	95,45	96,83	98,34	99,69	99,99	98,71	98,45	94,6	95,64		

Table 2

Core	C1																			
Sample	C1/90									C1/87										
cm bsf	88-90									86-87										
SiO_2	56,04	54,51	54,57	55,99	55,67	55,37	55,50	59,89	58,59	57,27	56,92	57,82	57,97	55,96	55,88	56,15	60,55	54,99	58,11	
TiO_2	1,97	1,83	1,86	1,59	1,61	1,94	1,55	2,02	1,61	1,60	1,64	1,88	1,77	1,26	1,67	1,78	1,05	1,84	1,34	
Al_2O_3	17,37	16,64	16,18	16,64	17,60	15,70	15,70	16,83	16,02	16,85	16,48	18,29	18,30	17,89	17,80	16,70	18,83	17,34	17,56	
FeO	5,53	8,13	9,59	7,78	7,77	8,28	8,79	4,53	5,91	7,76	6,60	6,21	6,82	7,62	7,88	7,92	4,64	7,45	5,92	
MnO	0,20	0,23	0,13	0,37	0,34	0,22	0,48	0,00	0,28	0,60	0,42	0,34	0,18	0,25	0,18	0,28	0,14	0,27	0,08	
MgO	1,19	2,29	2,33	2,12	2,15	2,32	2,04	1,03	1,57	1,38	2,08	0,89	0,77	1,28	1,58	1,40	0,97	2,44	1,19	
CaO	2,97	4,28	3,91	3,60	3,40	3,89	6,60	3,84	5,44	2,66	4,44	3,64	1,96	3,03	3,34	3,77	1,96	3,09	2,71	
Na_2O	7,31	5,75	5,15	5,26	5,54	5,73	5,76	6,08	6,44	5,03	5,55	5,44	4,67	5,90	5,05	5,04	5,77	6,34	6,15	
K_2O	5,54	4,95	4,43	4,76	4,20	4,94	2,13	4,56	2,82	5,29	4,75	4,24	6,53	4,98	4,73	4,73	4,65	4,44	5,26	
P_2O_5	1,51	1,00	1,14	1,18	1,28	1,60	1,19	1,11	1,14	1,00	0,71	0,77	0,46	1,29	1,17	1,45	0,70	1,18	1,13	
Cl	0,37	0,41	0,71	0,71	0,44	0,00	0,25	0,11	0,18	0,54	0,41	0,48	0,56	0,55	0,74	0,77	0,75	0,63	0,55	
Original Total	95,85	100,06	99,5	97,29	101,33	99,42	99,30	98,08	99,38	99,78	101,99	102,54	101,56	95,97	94,94	95,71	94,91	92,57	91,74	
Core	C1																			
Sample	C1/85a									C1/85b										
cm bsf	84-85																			
SiO_2	51,21	52,83	53,90	53,94	53,80	53,90	54,02	53,80	53,40	53,73	57,36	57,26	57,00	56,43	56,37	56,88	56,55	57,02	56,51	56,15
TiO_2	1,75	2,10	1,73	1,68	1,94	1,99	1,85	2,01	2,00	1,69	0,72	0,52	0,71	0,87	0,66	0,77	0,79	0,46	0,73	0,74
Al_2O_3	16,91	16,65	17,13	17,03	17,26	17,47	17,31	16,96	17,20	17,28	18,89	18,57	18,33	18,25	18,53	18,38	18,52	18,04	18,15	18,02
FeO	10,36	8,38	8,62	8,99	8,78	8,49	8,90	8,89	9,01	8,82	6,10	6,02	5,91	6,19	6,17	6,04	5,82	6,12	6,29	6,22
MnO	0,28	0,09	0,26	0,12	0,16	0,28	0,05	0,15	0,27	0,26	0,00	0,03	0,22	0,34	0,31	0,00	0,05	0,21	0,11	0,19
MgO	4,22	3,09	3,07	3,33	3,00	3,11	3,02	2,90	2,96	3,13	1,69	1,75	1,63	1,72	1,60	1,52	1,61	1,71	1,81	2,01
CaO	6,39	7,01	6,01	5,46	6,09	5,86	5,87	5,92	6,01	5,67	3,81	4,07	3,63	3,38	3,51	3,72	3,77	3,65	3,91	4,22
Na_2O	4,58	5,25	4,73	5,06	4,69	4,55	4,64	4,76	4,76	5,03	4,07	4,29	4,84	4,93	5,02	4,81	5,01	4,85	4,88	4,76
K_2O	3,26	3,42	3,19	3,11	3,11	3,06	3,09	3,29	3,14	3,19	6,57	6,68	6,96	7,08	6,91	7,02	7,32	7,12	6,87	6,88
P_2O_5	0,90	0,99	1,04	0,97	0,92	0,98	0,94	1,04	0,93	0,94	0,46	0,49	0,52	0,51	0,66	0,61	0,33	0,51	0,47	0,53
Cl	0,15	0,20	0,31	0,30	0,26	0,30	0,30	0,27	0,30	0,26	0,33	0,31	0,24	0,29	0,26	0,25	0,24	0,30	0,25	0,28
Original Total	95,99	95,86	95,33	96,31	99,73	96,6	96,63	98,57	95,46	96,13	98	95,84	94,4	96,32	95,48	95,34	95,23	97,16	97,07	95,75
Core	C1																			
Sample	C1/82									C1/56										
cm bsf	80-82									52-56										
SiO_2	56,23	54,73	55,02	55,92	55,02	56,46	55,95	56,37	54,61	54,49	54,80	54,55	54,54	55,88	55,51	55,52	54,96	54,70	54,90	55,15
TiO_2	1,87	1,94	1,99	1,67	2,03	2,02	1,77	1,81	0,33	0,49	0,49	0,47	0,39	0,09	0,41	0,25	0,50	0,56	0,30	0,14
Al_2O_3	16,89	16,16	15,97	17,11	16,74	17,58	18,45	17,22	19,80	20,96	21,30	21,36	20,38	21,18	22,32	22,05	22,58	20,51	21,71	22,35
FeO	7,36	8,89	10,00	8,66	8,99	7,61	8,29	6,53	4,31	3,56	2,93	3,27	3,80	3,40	2,45	2,02	2,57	4,16	2,72	2,24
MnO	0,26	0,27	0,29	0,23	0,39	0,03	0,10	0,34	0,00	0,28	0,32	0,06	0,17	0,00	0,00	0,07	0,33	0,17	0,00	0,06
MgO	1,92	2,26	2,06	1,59	2,12	1,71	1,18	1,46	0,71	0,46	0,51	0,52	0,54	0,63	0,12	0,07	0,12	0,67	0,29	0,14
CaO	3,48	4,04	3,31	3,63	3,62	2,64	2,25	2,52	5,53	5,17	3,71	4,07	4,94	4,38	2,59	3,04	3,15	4,22	3,54	2,94
Na_2O	6,33	5,55	5,19	5,24	5,07	6,03	5,81	6,54	5,53	6,12	5,53	5,77	5,04	5,60	6,73	7,32	6,74	5,01	7,08	6,75
K_2O	4,32	4,54	4,61	4,39	4,23	4,44	4,63	5,27	8,36	7,69	9,51	9,14	9,11	8,23	9,13	8,99	8,17	9,36	8,67	9,58
P_2O_5	1,23	1,52	1,11	1,03	1,08	1,01	0,98	1,41	0,00	0,12	0,30	0,00	0,31	0,06	0,00	0,00	0,17	0,00	0,00	0,00
Cl	0,10	0,10	0,46	0,52	0,71	0,46	0,59	0,53	0,82	0,66	0,61	0,79	0,77	0,55	0,74	0,66	0,70	0,63	0,79	0,65
Original Total	100,46	95,63	97,62	98,79	98,75	100,37	99,4	97,5	95,96	99,05	100,88	96,70	95,38	95,33	97,75	97,39	99,35	99,31	100,58	97,32

Table 2. Single glass chemistry for the studied tephra. All the analyses recalculated water free to 100. The original totals have been also reported.

Core	Sample	Lab No.	Sample type	Sampling depth from top of core (cm)	Depth of tephra from top of core (cm)	Radiocarbon age (a BP) 2σ	Calibrated age (cal a BP)
C1	C1/90-92	FI4084	mixed plank forams	90-92	80-90	3702±71	3625±96
AP1	GG0123	Poz-82785	G.*ruber*	7-8	12-13 cm	2590±30	2260±49
AP1	GG0130	Poz-82786	G.*ruber*	14-15		4570±35	4777±53
UM42	DD01317	UtC-8625	G.*ruber*	5.4-5.9	6.7-7.4	2202±41	1797±56
CP10BC	#25+#26	Poz-55177*	G.*ruber* and G.*sacculifer*	6–6.5	6.5-7	2280 ± 30	1890±44
CP10BC	#37+#38	Poz-74801	G.*ruber* and G.*sacculifer*	9-9.5		3255 ± 35	3075±60

Table 3. Summary of AMS ^{14}C datings on planktonic foraminifera extracted from cores samples. *from Wu *et al.* (2016).

Figure Captions:

Figure 1. Location of the studied cores (red full circles). All cores containing tephra related to the studied time span in the investigated area have been selected from the WDB-Paleo database and reported in the figure. Red (border) and orange (center) circles refer to cores cited in the text. Digital Terrain Model of the Naples Bay (inset B) courtesy of R. Tonielli. References: SW104-C5 in Margaritelli *et al.* (2016); C1201 and C1202 in Iorio *et al.* (2009), 2014; C1203 in Budillon *et al.*, (2012); C106 and C45 in Munno and Petrosino (2004); CET 1 in Morabito *et al.* (2014); MSK-12C4 in Cosentino *et al.* (2017); TIR2000-C01 in Di Roberto *et al.* (2008); KET80-11 and 80-03 in Paterne *et al.* (1988); GS1, D1, GT2 and GT4 in Crocitti *et al.* (2018); TEA C1-A in Pepe *et al.* (2018); TEA C6 in Di Donato *et al.* (2019); GT89-3 in Cini Castagnoli *et al.* (1990); Z1 in Geraga *et al.* (2008); CU12 set in Micallef *et al.* (2016); MS6 in Smedile *et al.* (2011); SW104_ND_14Q in Jalali *et al.* (2018); cores RF-, PAL-, IN68- and CM- in Calanchi *et al.* (1998) and Calanchi and Dinelli (2008); CSS00-12, CSS00-07, COS01-16 and AMC99-07 in Lowe *et al.* (2007); core MD90-917 in Siani *et al.* (2004); cores in Naples and Pozzuoli bays in Sacchi *et al.* (2005, 2014); cores in the Ionian Sea in Keller *et al.* (1978).

Figure 2. Entities recording data on tephra and cryptotephra in the WDB-Paleo database (Alberico *et al.*, 2017).

Figure 3. TAS classification diagrams (a-b) with composition of studied tephra and cryptotephra. Compositional fields are labelled according to the Na-and K-Series. The average compositional fields of proximal deposits and single glass data of some proximal and distal tephra are reported for comparison. Data for Somma-Vesuvius products are from Santacroce *et al.* (2008), Etna, Stromboli and Vulcano from Peccerillo (2005) and references therein, Cretaio from De Alteriis *et al.* (2010), FG proximal and Augusta Bay from De Martini *et al.* (2010) and Smedile *et al.* (2011), AAMS group from Smith *et al.* (2011), Upper Tufi di Grotte Rosse (UTGR) and TIR2000-50 from Albert *et al.* (2012), 8003-0 from Paterne *et al.* (1988), C6/199 from Di Donato *et al.* (2018), Pozzuoli Bay glasses from Sacchi *et al.* (2014), FG and FL from Coltelli *et al.* (2000, 2005); c) K_2O/Na_2O diagram to show the Na-alkaline affinity of studied cryptotephra and d) SiO_2/K_2O diagram to show the shoshonitic and HKCA features of cryptotephra CP10/7 and C1/85. Data for Salina and Lipari rhyolites from Albert *et al.* (2017).

Figure 4. SEM images of samples C1/90 and C1/85 to show a) the microlitic content of groundmass and the rare interstial glass of Etnean tephra, b) the two coexisting glass types with different morphologies in C1/85 and c) the porphyritic scoriae occurring with microlite bearing and aphyric glasses in tephra UM42/7.

Figure 5. Tephrostratigraphy of the studied records for the 4.4 ka-I Century AD time interval. Distal equivalents and source events from some cores in the southern Tyrrhenian, Gulf of Taranto and Adriatic Sea have been reported and discussed in the text. Reference cores may contain other tephra which have not been recalled here.

Figure 6. Binary diagrams with composition of tephra and cryptotephra compared with proximal counterparts and medial-distal equivalents; a) FeO_{tot} vs CaO diagram with tephra C14/89a and the 79 CE white and grey pumice from proximal site. Data from Santacroce *et al.* (2008), Sacchi *et al.* (2014) - Pozzuoli Bay tephra, Jalali *et al.* (2018) -ND14_Q/79, Di Donato *et al.* (2019) -C6/119, Lirer *et al.* (2013) - C90/232; b) SiO_2/FeO_{tot} vs TiO_2 and c) Na_2O/K_2O vs TiO_2 diagrams with composition of cryptotephra C1/85b, Stromboli (Secche di Lazzaro) and Vulcano (Palizzi A and UTGR) deposits and the marine TIR2000-50. Data from Albert *et al.* (2012, 2017); d) SiO_2 vs FeO_{tot} diagram with Etnean cryptotephra analyzed in this work and compared with mid and distal FG and FL equivalents. Single glass data from Sadori *et al.* (2013)- Pergusa Lake, Vogel *et al.* (2010)-OT07702-2 (Lake Ohrid), Caron *et al.* (2010)-Jo-42 (Lake Ohrid), Sulpizio *et al.* (2010)- SK13-514-average (Lake Shkodra), De Martini *et al*. (2010) and Smedile *et al*. (2011)-FG proximal and Augusta Bay.

Figure 7. Occurrences of major marker tephra in the Tyrrhenian, Adriatic and Ionian seas according to the results obtained here and integrated with those of the WdB-Paleo database. A number of terrestrial sites have been also included for AP, Avellino and AAMS deposits (Crocitti *et al.*, 2018 and references therein). The included two further findings of Avellino tephra in the Ionian Sea from the WdB-Paleo in addition to the SE and NW occurrences reported in Sulpizio *et al.* (2008, 2014) and Crocitti *et al.* (2018) allowed enlarging southward the dispersal of these products. Grey circles: core network investigated in this work; red full circles: study sites; coloured circles: occurrence of the marker tephra in the core network; red stars: source vents; *: marine age. °from Coltelli *et al.,* 2000. °°from Sevink *et al.* (2011) ^ from Lirer *et al.* (2013) for Agnano Monte Spina. ^^from Smith *et al.* (2011) for Astroni. For core references see Figure 1.

Figure 8. a) Occurrences of Cretaio, b) c) Lipari and Vulcano and d) e) Mt. Etna tephra and cryptotephra emplaced during the Late-Holocene. For the legend, see Figure 7.

Figure 9. Sketch map of isochrons for the Central Mediterranean Sea during the 4.4 ka - 79 AD time interval. Some continuous and age constrained lacustrine sequences have been included (e.g. Lake Monticchio: Wulf *et al.*, 2004; 2008; Lake Ohrid: Caron *et al.*, 2010; Lake Shkodra: Sulpizio *et al.*, 2010; Lake Nemi: Calanchi et al., 1996). The ~3.9 ka horizon corresponding to the Avellino event extends up to the Marmara Sea (Cagatay *et al.*, 2015). *: marine age from this study. Dashed lines link archives where the isochrons are inferred.

Table captions

Table 1. Summary of core and tephra data presented in this work including source volcano and event. Et: Etna, CF: Campi Flegrei, SV: Somma-Vesuvius, L: Lipari, Vulc: Vulcano; (1) age for Cretaio from Orsi *et al.* (1992); (2) De Alteriis *et al.* (2010); (3) Coltelli *et al.* (2000); (4) Smith *et al.* (2011); (5) Lirer *et al.* (2013); (6) Coltelli *et al.* (1998); (7) Di Donato *et al.* (2019). *Original sample code on board: AP1/13=GG0128, UM42/7=DD1320; CP10/7=CP10BC#14.

Table 2. Single glass chemistry for the studied tephra. All the analyses recalculated water free to 100. The original totals have been also reported.

Table 3. Summary of AMS ^{14}C datings on planktonic foraminifera extracted from cores samples. *from Wu *et al.* (2016).

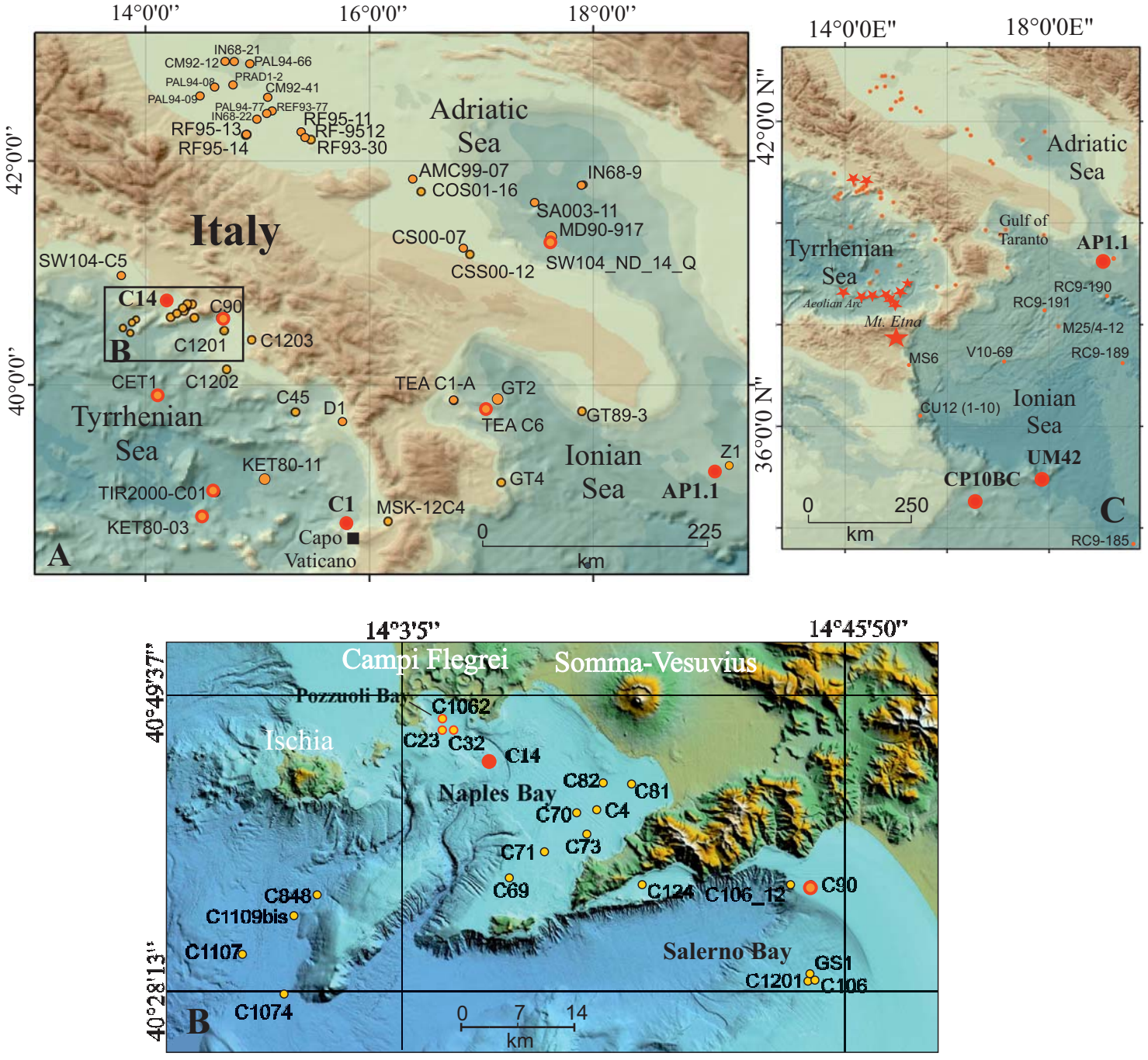
14°0'0''
16°0'0''
18°0'0''
42°0'0''
40°0'0''
IN68-21
CM92-12
PAL94-66
PAL94-08
PRAD1-2
CM92-41
PAL94-09
PAL94-77
REF93-77
IN68-22
RF95-11
RF95-13
RF-9512
RF95-14
RF93-30
Adriatic Sea
AMC99-07
IN68-9
COS01-16
SA003-11
MD90-917
Italy
CS00-07
SW104_ND_14_Q
CSS00-12
SW104-C5
C14
C90
B
C1201
C1203
CET1
C1202
TEA C1-A
GT2
C45
D1
TEA C6
GT89-3
Tyrrhenian Sea
Ionian Sea
Z1
KET80-11
GT4
AP1.1
TIR2000-C01
C1
MSK-12C4
KET80-03
Capo Vaticano
A
0
225
km
14°0'0E"
18°0'0E"
42°0'0 N"
36°0'0 N"
Adriatic Sea
Gulf of Taranto
AP1.1
Tyrrhenian Sea
RC9-190
Aeolian Arc
RC9-191
Mt. Etna
M25/4-12
MS6
V10-69
RC9-189
CU12 (1-10)
Ionian Sea
UM42
CP10BC
0
250
km
C
RC9-185
14°3'5"
14°45'50"
40°49'37"
40°28'13"
Campi Flegrei
Somma-Vesuvius
Pozzuoli Bay
C1062
Ischia
C23
C32
C14
C82
C81
Naples Bay
C70
C4
C71
C73
C69
C124
C106_12
C90
C848
C1109bis
C1107
Salerno Bay
GS1
C1201
C106
B
C1074
0
7
14
km

Figure 1

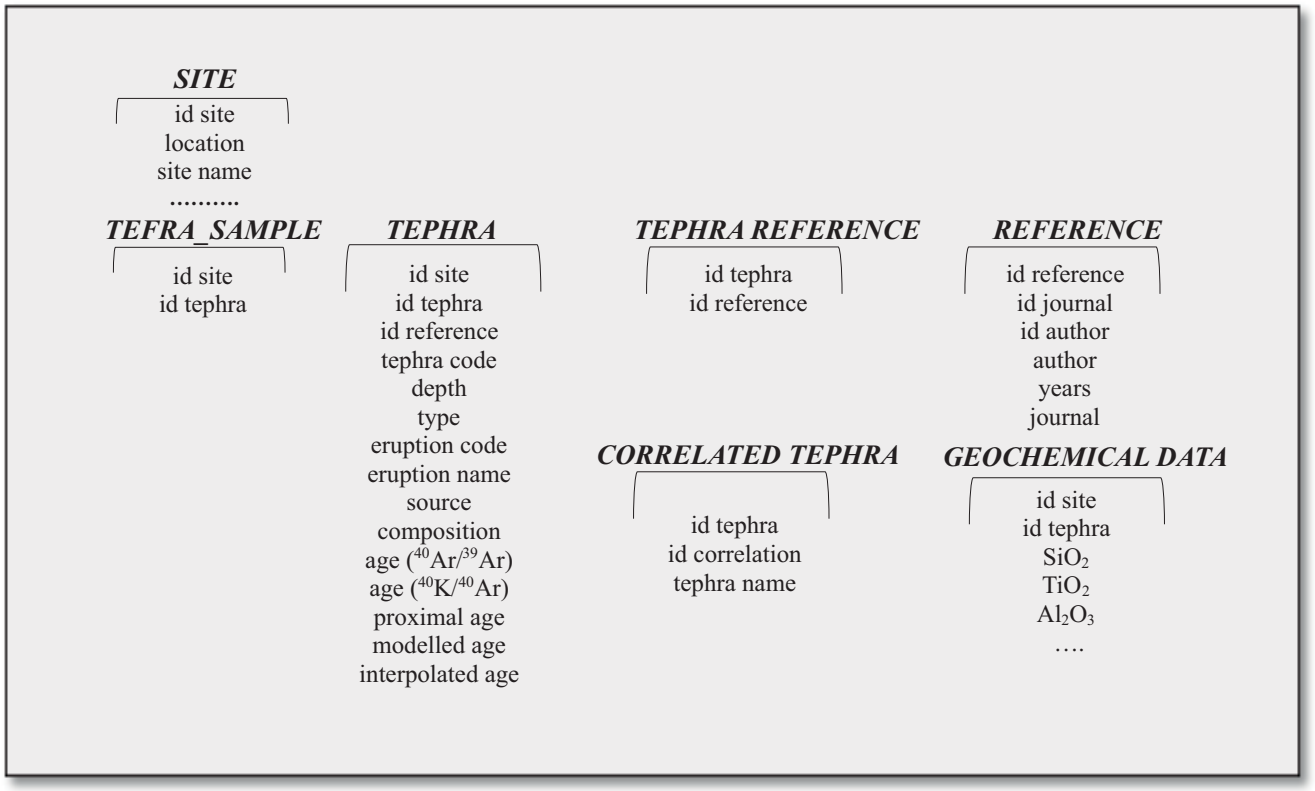
SITE
id site
location
site name
.....
TEFRA_SAMPLE
id site
id tephra
TEPHRA
id site
id tephra
id reference
tephra code
depth
type
eruption code
eruption name
source
composition
age ($^{40}Ar/^{39}Ar$)
age ($^{40}K/^{40}Ar$)
proximal age
modelled age
interpolated age
TEPHRA REFERENCE
id tephra
id reference
REFERENCE
id reference
id journal
id author
author
years
journal
CORRELATED TEPHRA
id tephra
id correlation
tephra name
GEOCHEMICAL DATA
id site
id tephra
SiO_2
TiO_2
Al_2O_3
….

Figure 2

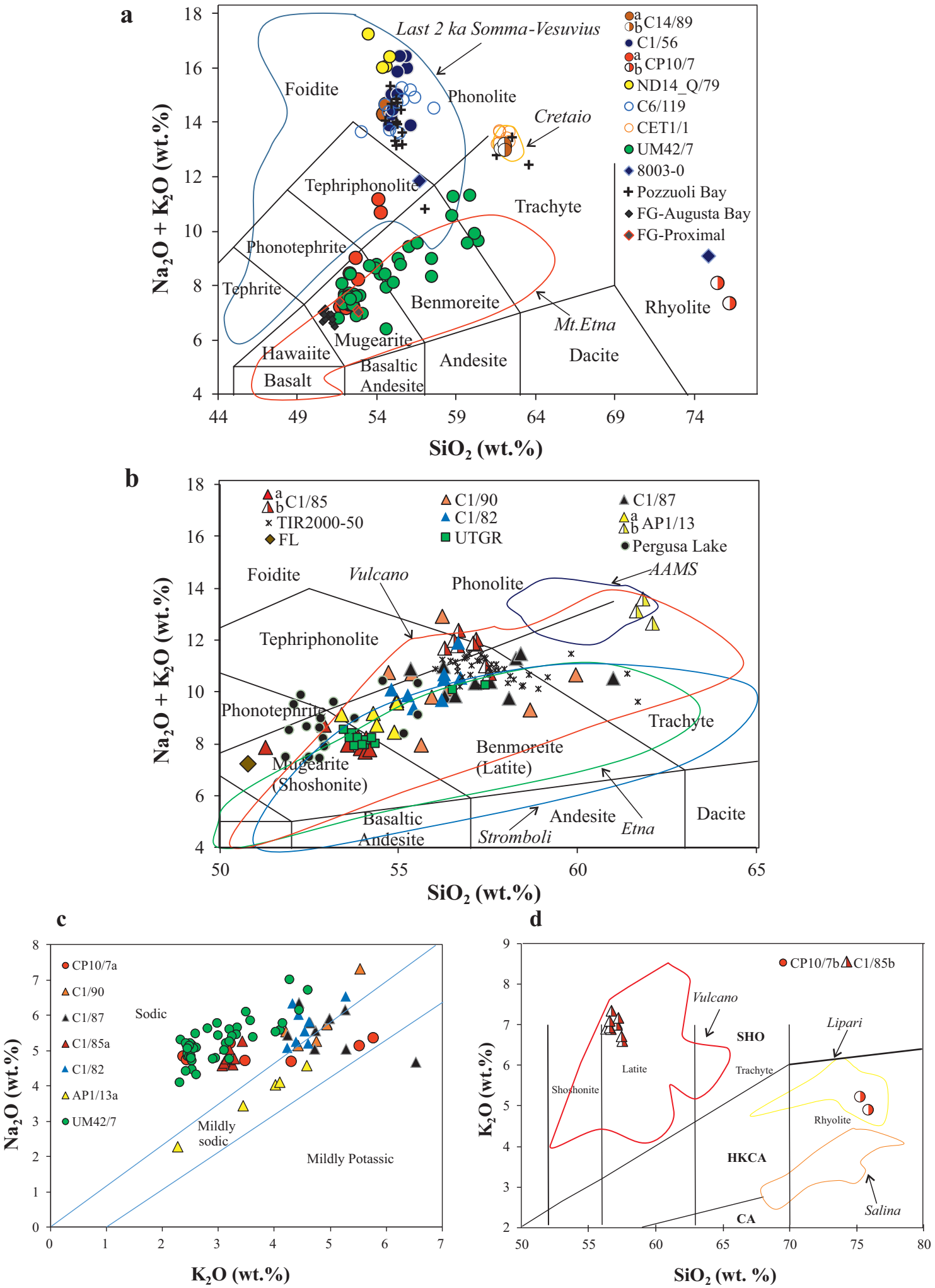
a
Last 2 ka Somma-Vesuvius
Foidite
Phonolite
Cretaio
Tephriphonolite
Trachyte
Phonotephrite
Tephrite
Benmoreite
Mt.Etna
Rhyolite
Mugearite
Hawaiite
Basaltic Andesite
Andesite
Dacite
Basalt
aC14/89
bC1/56
aCP10/7
bND14_Q/79
C6/119
CET1/1
UM42/7
8003-0
Pozzuoli Bay
FG-Augusta Bay
FG-Proximal
Na2O + K2O (wt.%)
SiO2 (wt.%)
b
aC1/85
TIR2000-50
FL
C1/90
C1/82
UTGR
C1/87
aAP1/13
bPergusa Lake
Foidite
Vulcano
Phonolite
AAMS
Tephriphonolite
Phonotephrite
Trachyte
Benmoreite (Latite)
Mugearite (Shoshonite)
Basaltic Andesite
Andesite
Etna
Stromboli
Dacite
Na2O + K2O (wt.%)
SiO2 (wt.%)
c
CP10/7a
C1/90
C1/87
C1/85a
C1/82
AP1/13a
UM42/7
Sodic
Mildly sodic
Mildly Potassic
Na2O (wt.%)
K2O (wt.%)
d
CP10/7b
C1/85b
Vulcano
Lipari
SHO
Latite
Trachyte
Shoshonite
Rhyolite
HKCA
CA
Salina
K2O (wt.%)
SiO2 (wt. %)

Figure 3

a)

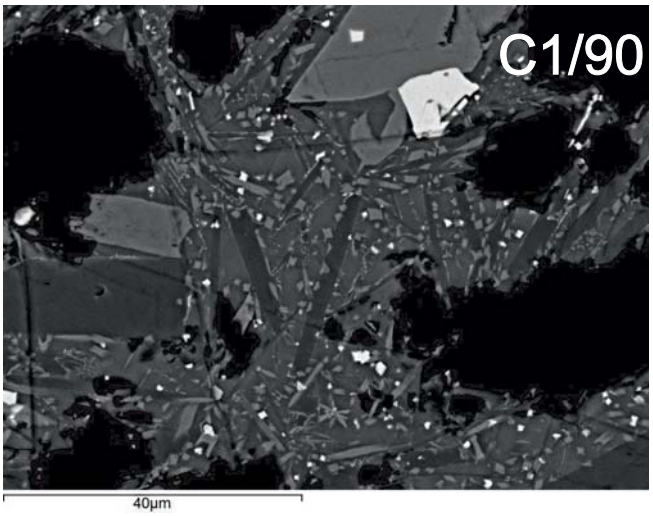

b)

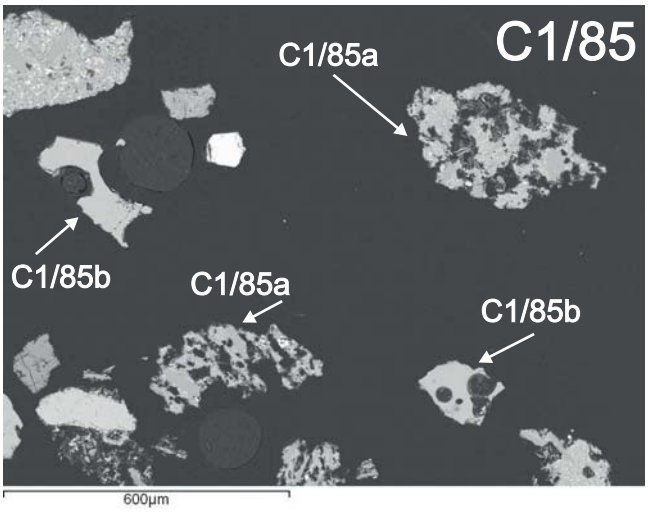

c)

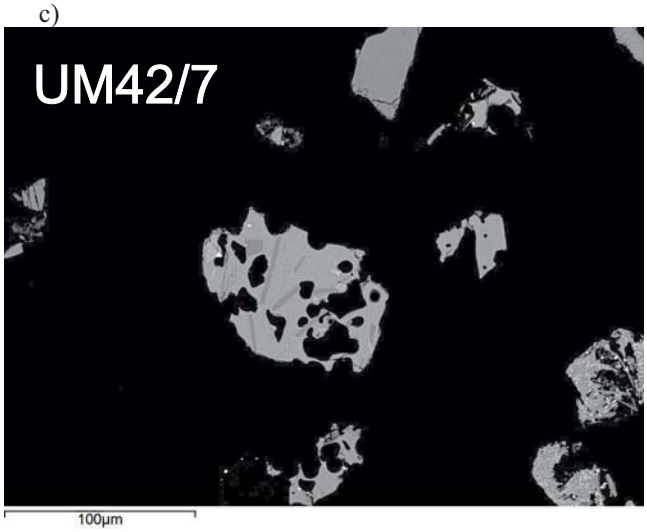

Figure 4

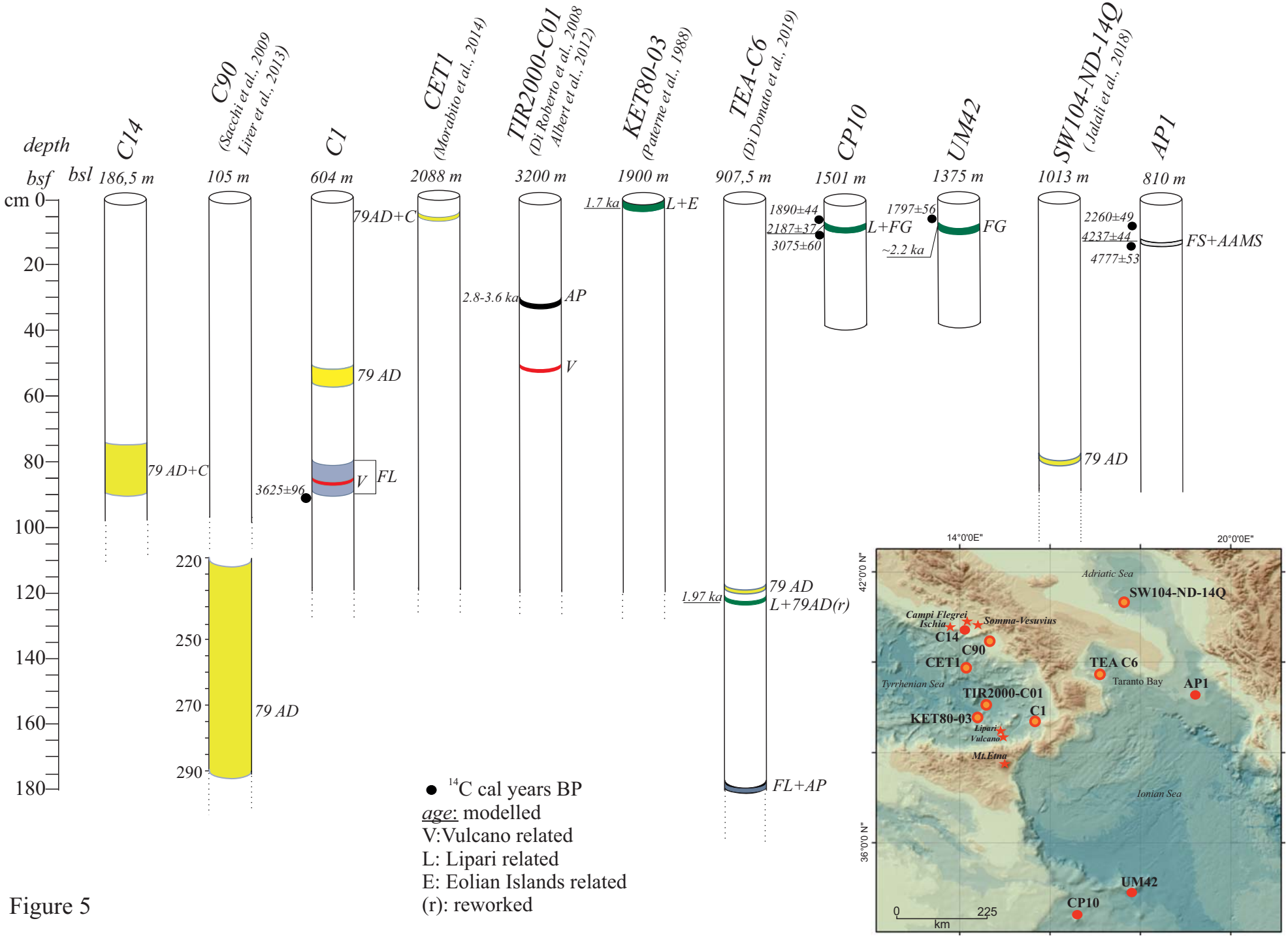
depth
bsf
bsl
cm 0
20
40
60
80
100
120
140
160
180
220
250
270
290
C14
186,5 m
79 AD+C
C90
(Sacchi et al., 2009
Lirer et al., 2013)
105 m
79 AD
C1
604 m
79AD+C
79 AD
3625±96
V
FL
CET1
(Morabito et al., 2014)
2088 m
TIR2000-C01
(Di Roberto et al., 2008
Albert et al., 2012)
3200 m
2.8-3.6 ka
AP
V
KET80-03
(Paterne et al., 1988)
1900 m
1.7 ka
L+E
TEA-C6
(Di Donato et al., 2019)
907,5 m
1.97 ka
79 AD
L+79AD(r)
FL+AP
CP10
1501 m
1890±44
2187±37
3075±60
L+FG
UM42
1375 m
1797±56
~2.2 ka
FG
SW104-ND-14Q
(Jalali et al., 2018)
1013 m
79 AD
AP1
810 m
2260±49
4237±44
4777±53
FS+AAMS
● 14C cal years BP
age: modelled
V:Vulcano related
L: Lipari related
E: Eolian Islands related
(r): reworked
14°0'0E"
20°0'0E"
42°0'0 N"
36°0'0 N"
Adriatic Sea
SW104-ND-14Q
Campi Flegrei
Ischia
Somma-Vesuvius
C14
C90
CET1
TEA C6
Taranto Bay
AP1
Tyrrhenian Sea
TIR2000-C01
C1
KET80-03
Lipari
Vulcano
Mt.Etna
Ionian Sea
UM42
CP10
0
225
km

Figure 5

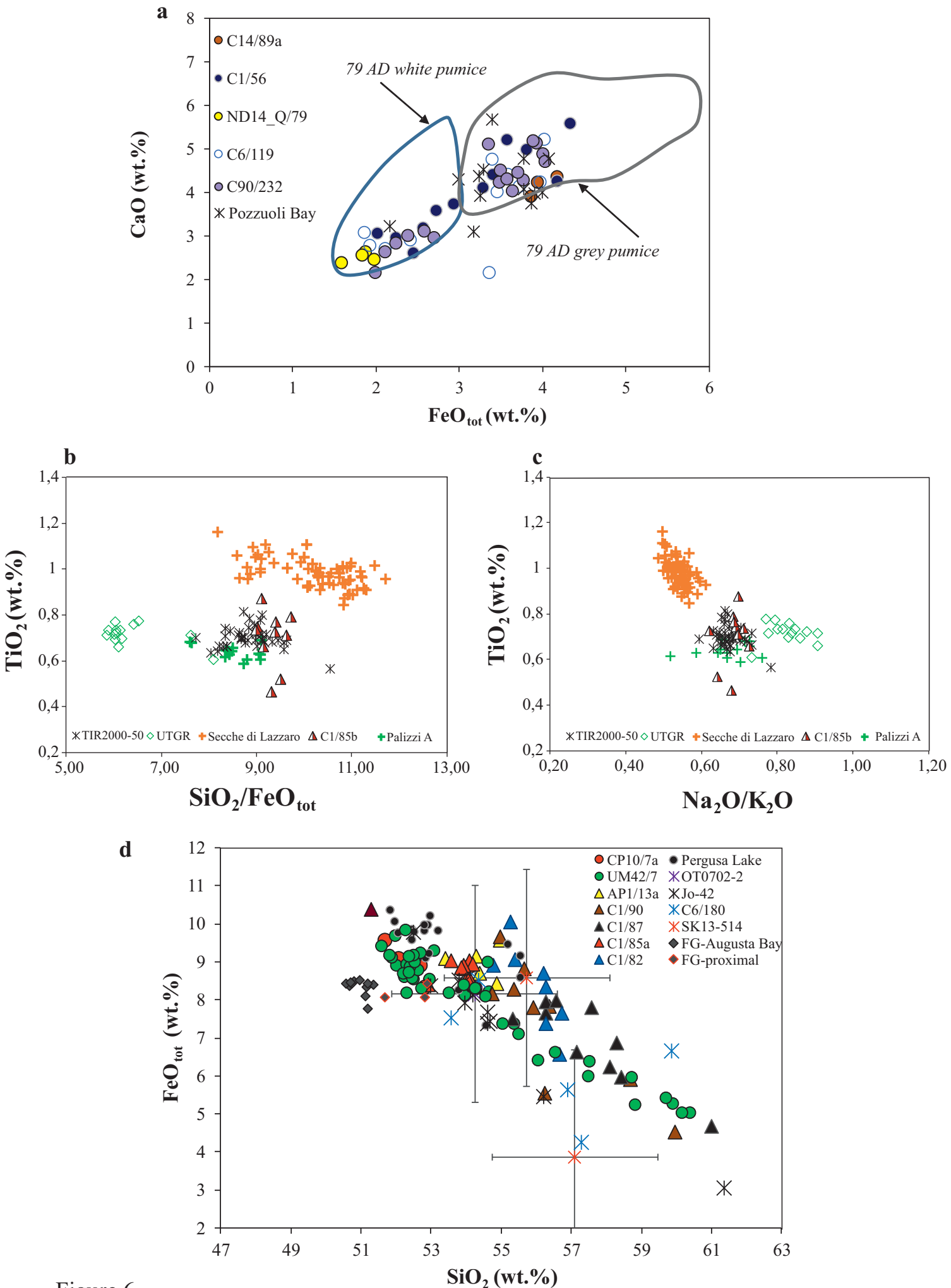
a
C14/89a
C1/56
ND14_Q/79
C6/119
C90/232
Pozzuoli Bay
79 AD white pumice
79 AD grey pumice
CaO (wt.%)
FeO tot (wt.%)
b
TiO2 (wt.%)
SiO2/FeO tot
TIR2000-50
UTGR
Secche di Lazzaro
C1/85b
Palizzi A
c
TiO2 (wt.%)
Na2O/K2O
d
CP10/7a
UM42/7
AP1/13a
C1/90
C1/87
C1/85a
C1/82
Pergusa Lake
OT0702-2
Jo-42
C6/180
SK13-514
FG-Augusta Bay
FG-proximal
FeO tot (wt.%)
SiO2 (wt.%)

Figure 6

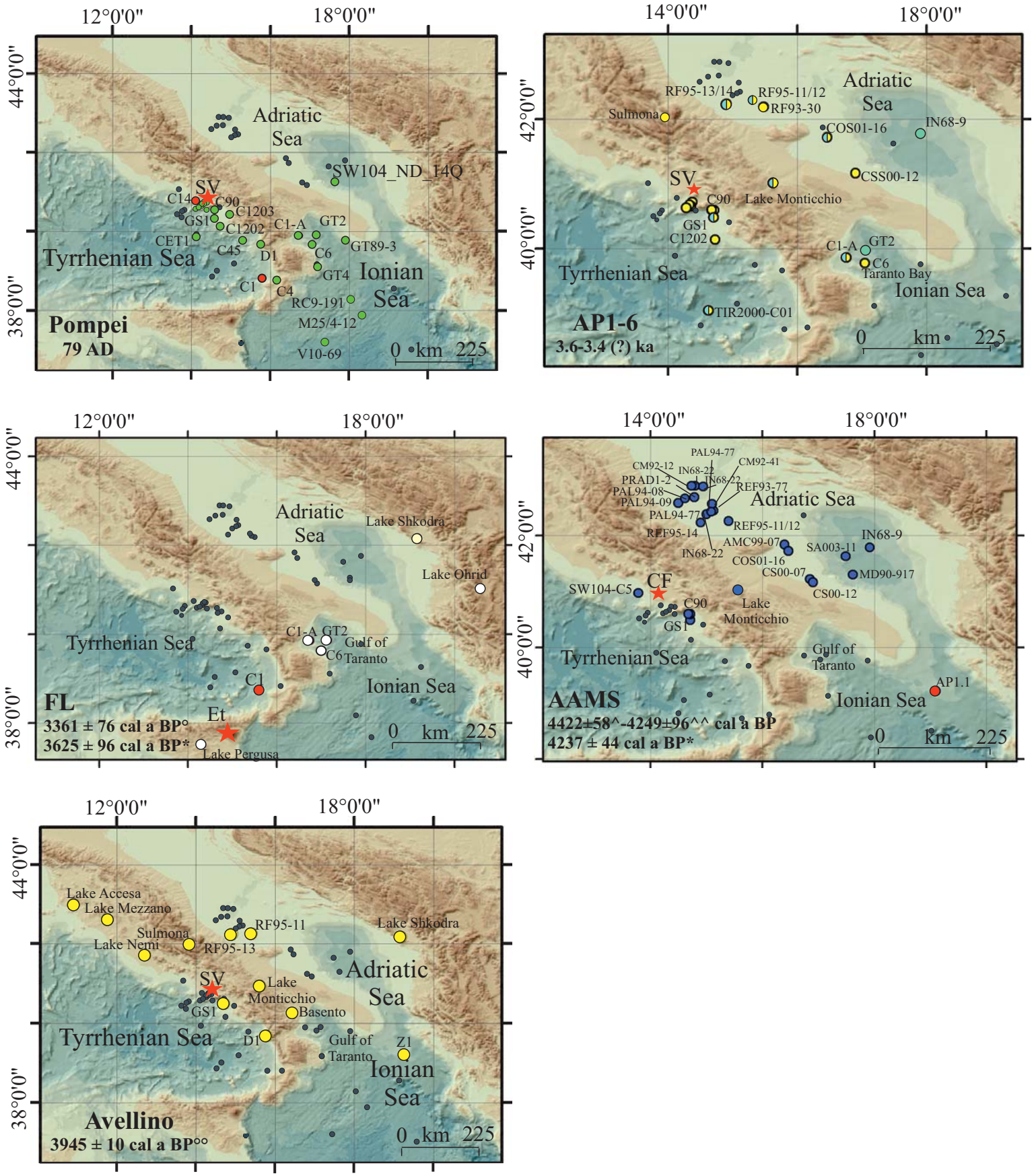
12°0'0"
18°0'0"
44°0'0"
38°0'0"
Adriatic Sea
SW104_ND_14Q
SV
C14
C90
C1203
GS1
C1202
C1-A
GT2
CET1
C45
D1
C6
GT89-3
Tyrrhenian Sea
GT4
Ionian Sea
C1
C4
RC9-191
M25/4-12
V10-69
Pompei
79 AD
0 km 225
14°0'0"
42°0'0"
40°0'0"
RF95-13/14
RF95-11/12
RF93-30
Sulmona
COS01-16
IN68-9
CSS00-12
Lake Monticchio
GS1
C1202
C1-A
GT2
C6
Taranto Bay
TIR2000-C01
AP1-6
3.6-3.4 (?) ka
Lake Shkodra
Lake Ohrid
Gulf of Taranto
FL
3361 ± 76 cal a BP°
3625 ± 96 cal a BP*
Et
Lake Pergusa
PAL94-77
CM92-12
IN68-22
CM92-41
PRAD1-2
REF93-77
PAL94-08
PAL94-09
REF95-14
REF95-11/12
AMC99-07
SA003-11
COS01-16
CS00-07
MD90-917
SW104-C5
CF
CS00-12
AP1.1
AAMS
4422±58^-4249±96^^ cal a BP
4237 ± 44 cal a BP*
Lake Accesa
Lake Mezzano
RF95-11
Lake Nemi
RF95-13
Lake Monticchio
Basento
Z1
Avellino
3945 ± 10 cal a BP°°

Figure 7

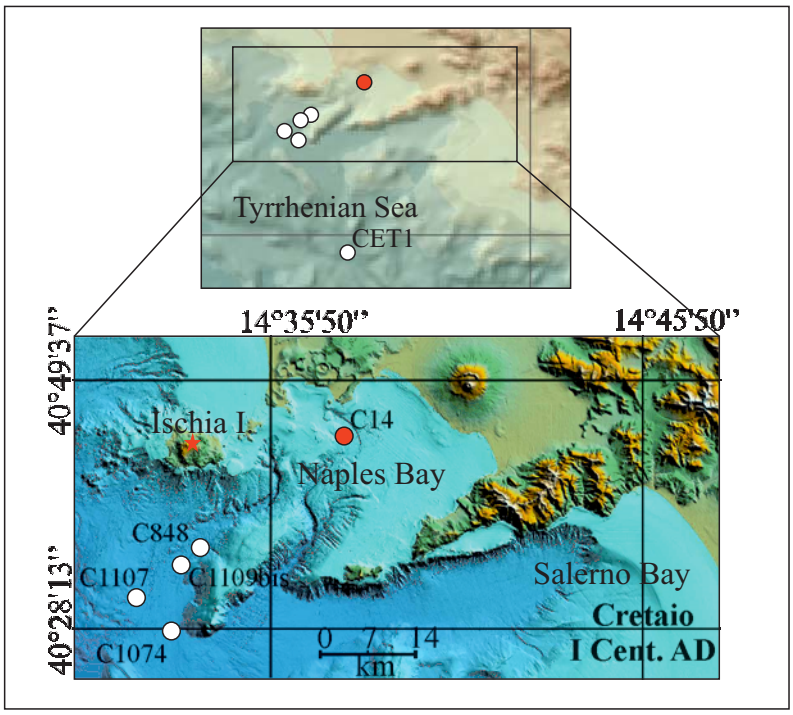
Tyrrhenian Sea
CET1
14°35'50"
14°45'50"
40°49'37"
40°28'13"
Ischia I.
C14
Naples Bay
C848
C1107
C1109bis
C1074
Salerno Bay
Cretaio
I Cent. AD
0 7 14
km

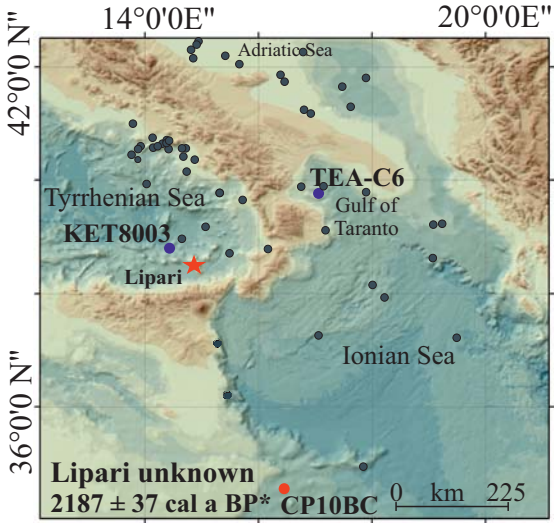
14°0'0E"
20°0'0E"
42°0'0 N"
36°0'0 N"
Adriatic Sea
Tyrrhenian Sea
TEA-C6
Gulf of Taranto
KET8003
Lipari
Ionian Sea
Lipari unknown
2187 ± 37 cal a BP*
CP10BC
0 km 225

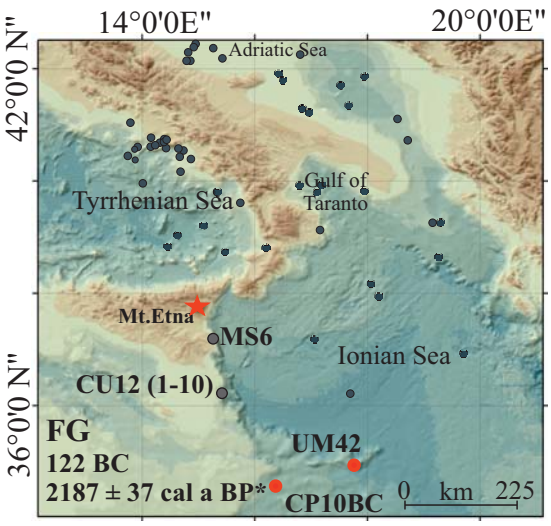
14°0'0E"
20°0'0E"
42°0'0 N"
36°0'0 N"
Adriatic Sea
Tyrrhenian Sea
Gulf of Taranto
Mt.Etna
MS6
Ionian Sea
CU12 (1-10)
FG
122 BC
2187 ± 37 cal a BP*
UM42
CP10BC
0 km 225

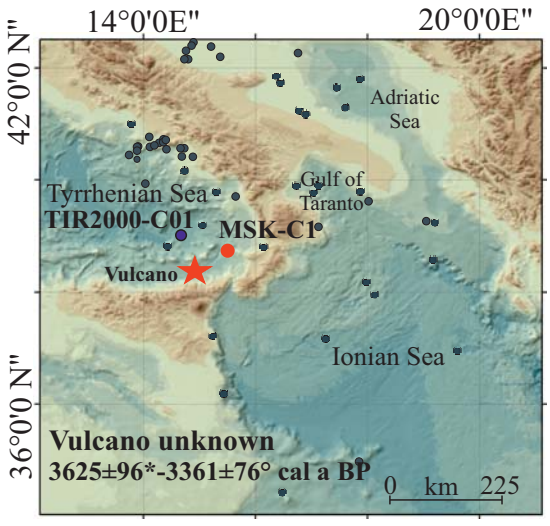
14°0'0E"
20°0'0E"
42°0'0 N"
36°0'0 N"
Adriatic Sea
Tyrrhenian Sea
Gulf of Taranto
TIR2000-C01
MSK-C1
Vulcano
Ionian Sea
Vulcano unknown
3625±96*-3361±76° cal a BP
0 km 225

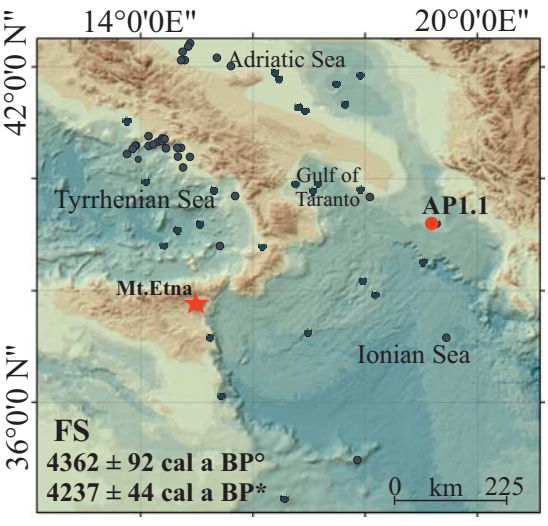
14°0'0E"
20°0'0E"
42°0'0 N"
36°0'0 N"
Adriatic Sea
Tyrrhenian Sea
Gulf of Taranto
AP1.1
Mt.Etna
Ionian Sea
FS
4362 ± 92 cal a BP°
4237 ± 44 cal a BP*
0 km 225

Figure 8

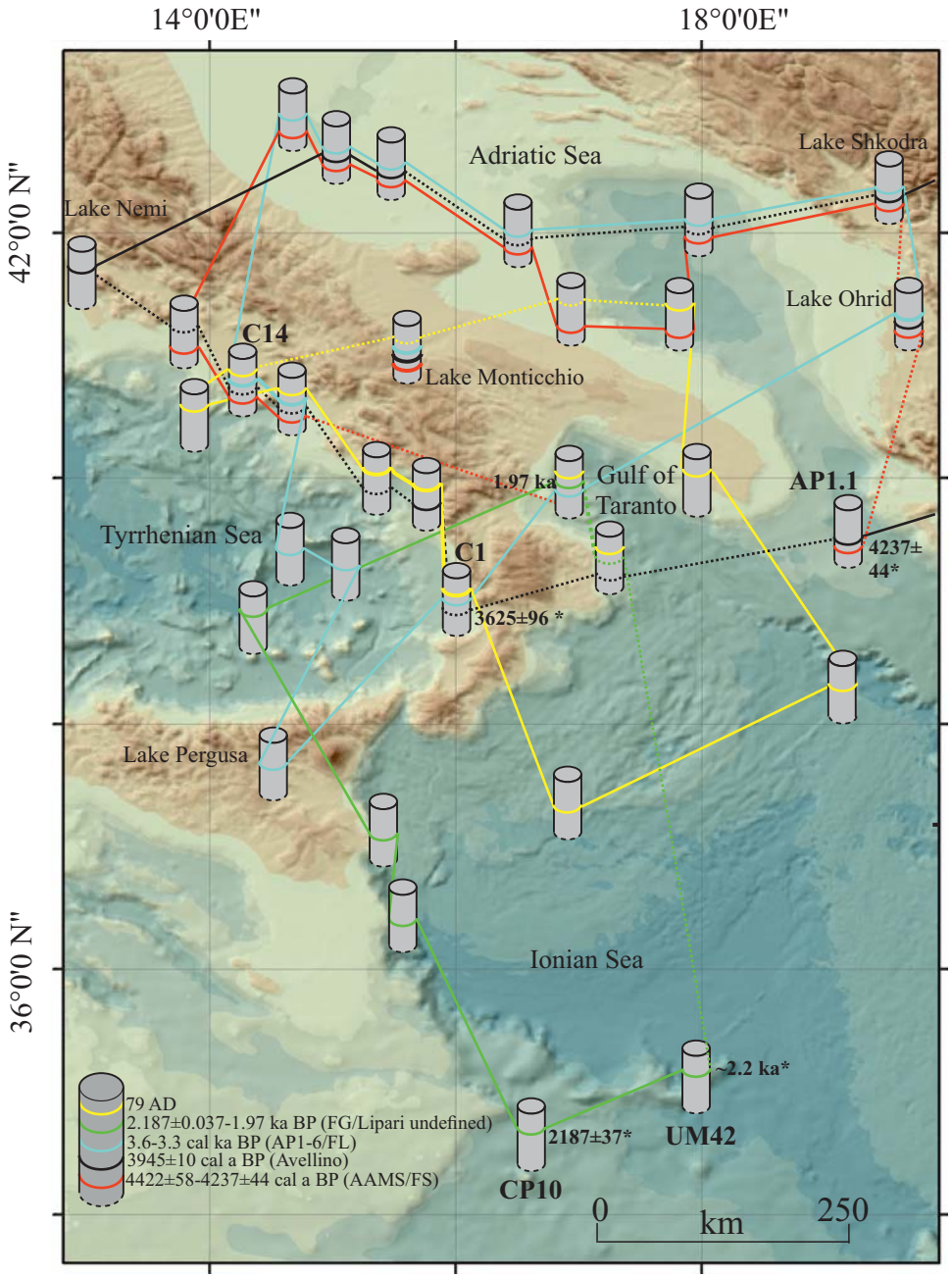
14°0'0E"
18°0'0E"
42°0'0 N"
36°0'0 N"
Adriatic Sea
Lake Shkodra
Lake Nemi
Lake Ohrid
C14
Lake Monticchio
1.97 ka
Gulf of
Taranto
AP1.1
Tyrrhenian Sea
C1
4237±
44*
3625±96 *
Lake Pergusa
Ionian Sea
~2.2 ka*
79 AD
2.187±0.037-1.97 ka BP (FG/Lipari undefined)
3.6-3.3 cal ka BP (AP1-6/FL)
3945±10 cal a BP (Avellino)
4422±58-4237±44 cal a BP (AAMS/FS)
2187±37*
UM42
CP10
0
km
250

Figure 9

Late Holocene tephra record of the central Mediterranean Sea: mapping occurrences and new potential isochrones for the 4.4-2.0 ka time interval

Insinga D.D.[1*], Petrosino, P. [2], Alberico I.[1], de Lange, G.J.[3], Lubritto, C.[4], Molisso F.[1], Sacchi M.[1], Sulpizio, R.[5], Wu, J.[3,6] & Lirer F.[1]

[1]Istituto di Scienze Marine (ISMAR)-CNR, Calata Porta di Massa, Interno Porto di Napoli, Napoli

[2]Dipartimento di Scienze della Terra dell'Ambiente e delle Risorse (DiSTAR), Università degli Studi "Federico II" di Napoli

[3]Department of Earth Sciences-Geochemistry, Utrecht University, The Netherlands

[4]Dipartimento di Scienze e Tecnologie Ambientali, Biologiche e Farmaceutiche, Università della Campania "Luigi Vanvitelli", Caserta

[5]Dipartimento di Scienze della Terra e Geoambientali, Università di Bari

[6]State Key Laboratory of Marine Geology, Tongji University, China

*corresponding author

e-mail: donatelladomenica.insinga@cnr.it

Contents

Secondary Standards

	SiO_2	TiO_2	Al_2O_3	FeOt*	MnO	MgO	CaO	Na_2O	K_2O	P_2O_5	Cl	F	SO_2	H_2O	total
	ryolithic Lipari obsidian ID3506														
	74,10	0,07	13,10	1,55	0,06	0,04	0,73	4,07	5,11	0,01	0,34	0,15	0,00	0,65	100,03
LO1	74,07	0,00	13,33	1,46	0,10	0,04	0,69	3,92	5,03	0,01	0,40	n.d	n.d		99,05
LO2	73,74	0,22	13,03	1,64	0,14	0,10	0,63	4,08	5,13	0,00	0,40	n.d	n.d		99,11
LO3	73,90	0,14	13,29	1,48	0,08	0,10	0,70	4,09	5,19	0,00	0,32	n.d	n.d		99,29
LO4	72,95	0,06	12,99	1,66	0,09	0,04	0,68	4,19	5,12	0,02	0,34	n.d	n.d		98,14
LO5	74,10	0,00	13,25	1,83	0,14	0,00	0,74	4,01	5,23	0,00	0,37	n.d	n.d		99,67
LO6	73,44	0,18	13,53	1,51	0,00	0,06	0,69	4,00	5,15	0,02	0,38	n.d	n.d		98,96
LO7	74,22	0,12	13,38	1,59	0,08	0,02	0,66	4,07	5,17	0,04	0,40	n.d	n.d		99,75
LO8	74,26	0,00	13,25	1,50	0,06	0,05	0,72	4,17	5,18	0,00	0,38	n.d	n.d		99,57
LO9	73,81	0,00	13,20	1,52	0,11	0,10	0,78	4,23	5,13	0,02	0,35	n.d	n.d		99,25
LO10	74,08	0,04	13,29	1,39	0,00	0,04	0,83	4,10	5,27	0,00	0,30	n.d	n.d		99,34
LO11	73,77	0,20	13,39	1,57	0,19	0,06	0,65	4,10	5,08	0,05	0,34	n.d	n.d		99,40
LO12	73,39	0,08	13,13	1,56	0,02	0,12	0,81	4,13	5,09	0,00	0,27	n.d	n.d		98,60
LO13	74,09	0,22	13,15	1,50	0,14	0,01	0,70	4,11	4,99	0,00	0,37	n.d	n.d		99,28
LO14	74,12	0,13	13,15	1,61	0,02	0,08	0,78	4,20	5,23	0,03	0,32	n.d	n.d		99,67
LO15	73,95	0,00	13,41	1,58	0,18	0,14	0,58	4,17	5,06	0,06	0,37	n.d	n.d		99,50

	SiO_2	TiO_2	Al_2O_3	FeOt*	MnO	MgO	CaO	Na_2O	K_2O	P_2O_5	Cl	F	SO_2	H_2O	Analythical total
	Basaltic Laki 1783 A.D. tephra														
	49,70	3,08	13,00	14,10	0,23	5,39	9,70	2,85	0,46	0,35	0,02	0,11	0,09		99,09
BLA 1	49,53	3,01	13,02	14,06	0,29	5,22	9,82	2,97	0,60	0,28	0,01	n.d	n.d		98,81
BLA 2	49,31	3,06	13,43	14,12	0,30	5,45	9,70	3,09	0,55	0,38	0,00	n.d	n.d		99,39
BLA 3	49,24	2,80	13,09	14,10	0,39	5,53	9,86	2,91	0,57	0,45	0,01	n.d	n.d		98,95
BLA 4	49,95	3,05	13,50	14,17	0,16	5,52	9,73	3,01	0,53	0,30	0,00	n.d	n.d		99,92
BLA 5	49,84	2,83	13,13	13,96	0,36	5,53	9,66	2,93	0,54	0,25	0,04	n.d	n.d		99,07
BLA 6	49,86	3,11	13,49	14,04	0,14	5,44	9,83	2,95	0,56	0,36	0,01	n.d	n.d		99,79
BLA 7	50,15	3,00	13,39	14,04	0,28	5,55	9,97	2,99	0,48	0,44	0,00	n.d	n.d		100,29
BLA 8	49,47	2,87	13,12	14,22	0,29	5,49	9,65	2,81	0,53	0,43	0,03	n.d	n.d		98,91
BLA 9	48,98	3,02	12,91	13,96	0,38	5,55	9,50	2,81	0,64	0,14	0,01	n.d	n.d		97,90
BLA 10	49,50	3,01	12,89	13,99	0,32	5,41	9,81	3,12	0,59	0,31	0,04	n.d	n.d		98,99
BLA 11	48,79	3,10	13,04	14,07	0,20	5,55	9,55	2,70	0,56	0,41	0,00	n.d	n.d		97,97
BLA 12	49,64	3,04	13,13	13,96	0,25	5,56	9,63	2,79	0,50	0,33	0,03	n.d	n.d		98,86
BLA 13	48,89	3,11	13,06	13,93	0,26	5,57	9,67	2,85	0,51	0,41	0,00	n.d	n.d		98,26
BLA 14	48,82	3,12	13,09	14,52	0,17	5,44	9,85	3,01	0,46	0,39	0,04	n.d	n.d		98,91
BLA 15	49,33	3,11	12,87	14,16	0,42	5,27	9,72	2,99	0,66	0,32	0,00	n.d	n.d		98,85
BLA 16	49,01	2,96	13,16	14,03	0,47	5,36	9,70	3,05	0,55	0,29	0,00	n.d	n.d		98,58
BLA 17	49,31	3,16	12,88	14,14	0,30	5,47	9,75	3,00	0,50	0,32	0,00	n.d	n.d		98,83
BLA 18	49,46	3,12	13,03	14,26	0,35	5,72	9,57	2,74	0,58	0,31	0,01	n.d	n.d		99,15
BLA 19	49,30	3,13	13,24	13,83	0,17	5,52	9,72	3,04	0,57	0,26	0,04	n.d	n.d		98,82
BLA 20	49,51	3,37	13,07	13,91	0,35	5,48	9,92	2,88	0,52	0,41	0,01	n.d	n.d		99,43
BLA 21	49,51	3,08	12,94	14,63	0,07	5,44	9,57	2,86	0,54	0,42	0,06	n.d	n.d		99,12

Table S1. Results of the analytical routine of secondary standards Lipari rhyolitic obsidian ID3506 and Laki basalt (Kuehn et al., 2011) acquired in the same operating conditions of the unknown samples.* All Fe reported as FeO. N.d.: not determined.

Reference

Kuehn SC, Froese DG, Shane PAR et al. 2011. The INTAV intercomparison of electron-beammicroanalysis of glass by tephrochronology laboratories: results and recommendations. Quaternary International 246: 19–47.

A

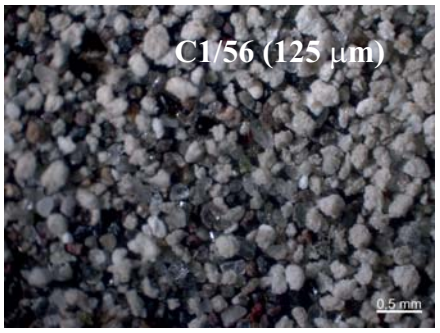

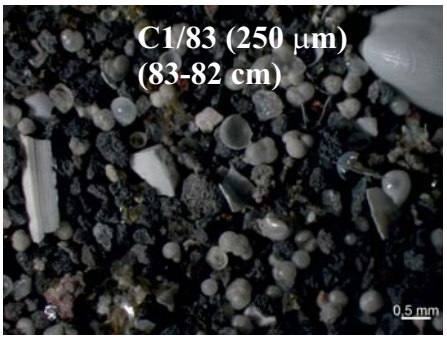

N.A.

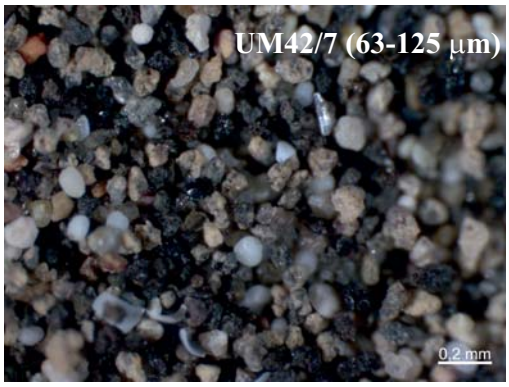

N.A.

A

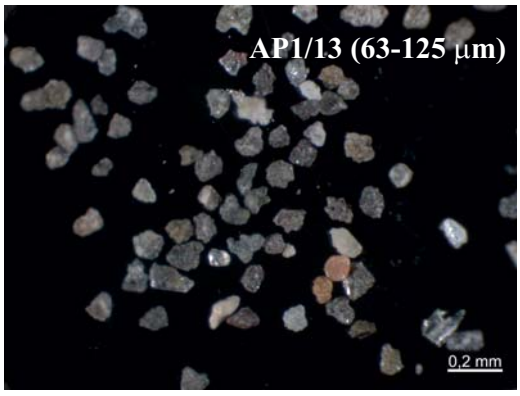

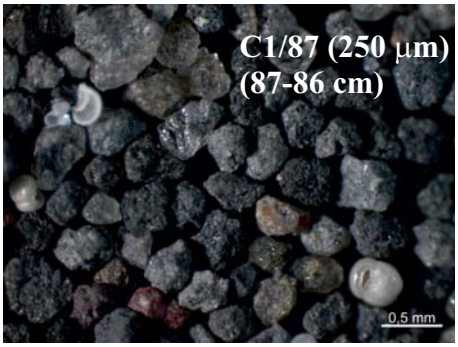

A

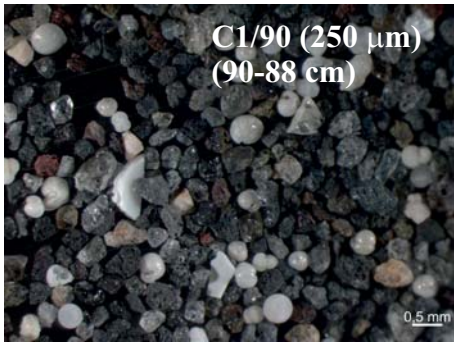

A

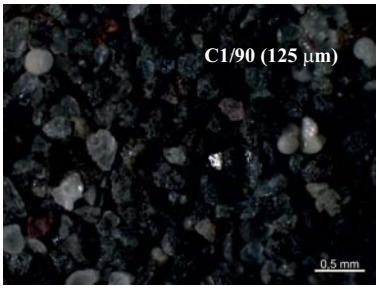

Fig. S1. Photographs at the optical microscope of tephra UM42/7 and cryptotephra. The images of subsamples taken from the cryptotephra dispersed between 90 and 80 cm bsf in core C1 are reported to show the variable proportions of volcanic and biotic fractions along the stratigraphic height. A: analyzed; N.A.: not analyzed.

Event	^{14}C (a)	±	cal ^{14}C (2 sigma)	cal ^{14}C (1 sigma)	mean value (μ) ± standard deviation (σ)	material	**modelled**/varve age of tephra (cal a BP)	historical age	references	notes
Cretaio	1970	70	165 BC-213 AD	48 BC -123 AD	23 ± 87 AD	humic acid in underlying paleosol			Orsi et al., 1992	consistent with stratigraphic evidences
	1750	70	87-423 AD	217-388 AD	278 ± 85 AD					
	2332	24	85 BC-83 AD	36 BC-45 AD	3 ± 42 AD	forams 1 cm below the tephra offshore Ischia island			De Alteriis et al., 2010	consistent with stratigraphic evidences
FG	2180	60	384 BC-61 BC	359 BC-172 BC	243 ± 85 BC	paleosol between lava and fall at Trecastagni				
	2030	70	339 BC-126 AD	153 BC-52 AD	54 ± 92 BC	paleosol between lava and fall at other site			Coltelli et al., 1998	
	2040	60	202 BC-80 AD	156 BC-24 AD	62 ± 80 BC	paleosol between lava and fall at other site		122 BC		
	2202	41	43-260 AD	93-208 AD	153 ± 56 AD	forams 1 cm above UM42/7	**ca. 2.2 ka**			
	2280	30	32 BC-145 AD	15-105 AD	60 ± 44 AD	forams 0.5 cm above CP10/7			this study	
	3255	35	3195-2953 cal a BP	3145-3018 cal a BP	3075 ± 60 cal a BP	forams 2.5 cm below CP10/7	**2187 ± 37**			
FL	3150	60	3550-3210 cal a BP	3448-3260 cal a BP	3361 ± 76 cal a BP	charred material			Coltelli et al., 2000	
	3055	75	3446-3037 cal a BP	3360-3170 cal a BP	3245 ± 99 cal a BP	sediment below tephra FL in Lake Pergusa			Sadori and Narcisi, 2001	
	3702	71	3818-3444 cal a BP	3715-3520 cal a BP	3625 ± 96 cal a BP	forams below the tephra in Marisk C-1			this study	
FS	3930	60	4525-4159 cal a BP	4497-4257 cal a BP	4362 ± 92 cal a BP	charred material			Coltelli et al., 2000	
	2590	30	2337-2159 cal a BP	2324-2209 cal a BP	2260 ± 49 cal a BP	forams 5.5 cm above tephra AP1/13				
	4570	35	4859-4650 cal a BP	4837-4724 cal a BP	4777 ± 53 cal a BP	forams 1.5 cm below tephra AP1/13	**4237 ± 44**		this study	
AP6								217/216 BC?	Santacroce et al., 2008 and references therein	
	3559	46	3566-3343 cal a BP	3505-3384 cal a BP	3452 ± 59 cal a BP	forams 10 cm above tephra AP6 in the Salerno Bay	**3484 ± 36**		Lirer et al., 2013	
AP5							3940±200		Wulf et al., 2008	
AP4							3990±200		Wulf et al., 2004	
AP3	2710	60	2945-2746 cal a BP	2855-2759 cal a BP	2827 ± 55 cal a BP	charcoal interbedded within AP3 products or in the underlying paleosol			Rolandi et al., 1998	
							3588 ± 50		Lirer et al., 2013	
							4020±200		Wulf et al., 2004	
AP2	3380	23	3690-3572 cal a BP	3677-3587 cal a BP	3625 ± 32 cal a BP	bone above AP2			Passariello et al., 2010	
	3300	80	3720-3363 cal a BP	3632-3448 cal a BP	3538 ± 93 cal a BP					
	3400	160	4138-3255 cal a BP	3845-3455 cal a BP	3678 ± 201 cal a BP				Santacroce et al., 2008 and references therein	
	3000	200	3640-2750 cal a BP	3395-2925 cal a BP	3181 ± 238 cal a BP					
	3280	70	3686-3371 cal a BP	3585-3410 cal a BP	3514 ± 79 cal a BP					
	3250	70	3677-3345 cal a BP	3561-3401 cal a BP	3484 ± 79 cal a BP	charcoal interbedded within AP2 products or in the underlying paleosol			Rolandi et al. 1998	
	3150	100	3606-3077 cal a BP	3475-3231 cal a BP	3356 ± 126 cal a BP					
							4150±210		Wulf et al., 2004	
AP1	3361	20	3680-3564 cal a BP	3632-3576 cal a BP	3606 ± 28 cal a BP	bone above AP1				
	3368	47	3809-3476 cal a BP	3689-3562 cal a BP	3610 ± 65 cal a BP	bone above AP1			Passariello et al., 2010	
	3399	37	3820-3562 cal a BP	3692-3593 cal a BP	3649 ± 53 cal a BP	bone above AP1				
	3368	19	3683-3569 cal a BP	3634-3584 cal a BP	3612 ± 27 cal a BP	charcoal above AP1				
	3270	50	3609-3386 cal a BP	3809-3595 cal a BP	3682 ± 68 cal a BP					
	3220	65	3607-3260 cal a BP	3556-3375 cal a BP	3451 ± 75 cal a BP				Santacroce et al., 2008 and references therein	
	3279	60	3639-3381 cal a BP	3577-3447 cal a BP	3511 ± 68 cal a BP	charcoal interbedded within AP1 products or in the underlying paleosol				
	3500	60	3959-3616 cal a BP	3846-3694 cal a BP	3774 ± 78 cal a BP				Rolandi et al., 1998	
Avellino	3550	20	3901-3727 cal a BP	3883-3830 cal a BP	3840 ± 41 cal a BP	goat bone buried by Avellino				
	3513	20	3850-3707 cal a BP	3836-3725 cal a BP	3778 ± 40 cal a BP	bone above Avellino			Passariello et al., 2010	
	3597	22	3971-3842 cal a BP	3959-3867 cal a BP	3904 ± 35 cal a BP	bone below Avellino				
					3945 ± 10 cal a BP				Sevink et al., 2011	mean of 20 age datings
	3530	40	3920-3694 cal a BP	3870-3724 cal a BP	3803 ± 61 cal a BP	charcoal in the Avellino pumice fall (Lagno Grado)			Zanchetta et al., 2011	
	3820	40	4406-4091 cal a BP	4288-4149 cal a BP	4225 ± 77 cal a BP	bulk sediment above Avellino tephra in the Lake Mezzano			Zanchetta et al., 2011	
	3960	60	4777-4184 cal a BP	4520-4297 cal a BP	4411 ± 98 cal a BP				Santacroce et al., 2008	
							4310 ± 220		Wulf et al., 2008 and references therein	
Astroni							**4153-4345**		Smith et al., 2011 and references therein	
	3900	40	4430-4161 cal a BP	4415-4290 cal a BP	4331 ± 63 cal a BP				Zanchetta et al., 2011	
	3780	70	4407-4980 cal a BP	4284-3997 cal a BP	4166 ± 114 cal a BP	forams in the tephra			Siani et al., 2004	
							4660 ± 230		Wulf et al., 2004	
AMS							**4482-4625**		Smith et al., 2011 and references therein	
	4382	32	4796-4333 cal a BP	4650-4410 cal a BP	4546 ± 119 cal a BP	forams 2 cm below AMS tephra	**4422 ± 58**		Lirer et al., 2013	
							5390 ± 270		Wulf et al., 2008	

Table S2. Selected chronological data at both proximal and distal (marine and lacustrine) sites published for some of the investigated tephra. All the 14C dates were converted into calendar ages using the IntCal13 and Marine13 calibration curve (Reimer et al., 2013) implemented in the program OxCal 4.3 (Bronk Ramsey, 2009) with no regional reservoir correction (i.e. ΔR=0), which is valid for the modern Mediterranean (Siani et al., 2000). Interpolated ages are proposed for AP1/13 and CP10/7 using the OxCal U_Sequence function (" ", 10) developed for the short stratigraphic intervals constrained by radiocarbon datings and using the "Date" command.

Supplementary Table 2 References

Bronk Ramsey C 2009. Bayesian Analysis of Radiocarbon Dates. Radiocarbon 51: 337–360.

Coltelli M, Del Carlo P, Vezzoli L 1998. Discovery of a Plinian basaltic eruption of Roman age at Etna volcano, Italy. Geology 26: 1095–1098.

Coltelli M, Del Carlo P, Vezzoli L 2000. Stratigraphic constraints for explosive activity in the past 100 ka at Etna Volcano, Italy. International Journal of Earth Sciences 89: 665–677.

De Alteriis G, Insinga D, Morabito S et al. 2010. Age of submarine debris avalanches and tephrostratigraphy offshore Ischia Island, Tyrrhenian Sea, Italy. Marine Geology 278: 1-18.

Lirer F, Sprovieri M, Ferraro L, et al. 2013. Integrated stratigraphy for the Late Quaternary in the eastern Tyrrhenian Sea. Quaternary International 292: 71-85

Orsi G, Gallo G, Heiken G et al 1992. A comprehensive study of pumice formation and dispersal: the Cretaio Tephra of Ischia (Italy). Journal of Volcanology and Geothermal Research 53: 329-354.

Passariello I, Lubritto C, D'Onofrio A et al. 2010. The Somma–Vesuvius complex and the Phlaegrean Fields caldera: New chronological data of several eruptions of the Copper–Middle Bronze Age period. Nuclear Instruments and Methods in Physics Research B 268: 1008–1012.

Reimer PJ, Bard E, Bayliss A et al. 2013. IntCal13 and Marine13 Radiocarbon Age Calibration Curves 0–50,000 Years cal BP. Radiocarbon 55: 1869–1887.

Rolandi G, Petrosino P, Mac Geehin J 1998. The interplinian activity at Somma–Vesuvius in the last 3500 years. Journal of Volcanology and Geothermal Research 82:19-52.

Sadori L, Narcisi B, 2001. The postglacial record of environmental history from Lago di Pergusa, Sicily. Holocene 11 (6): 655–670.

Santacroce R, Sulpizio R, Zanchetta G et al 2008. Age and whole rocks-glass composition of proximal pyroclastics from the major explosive eruptions of Vesuvius: a review as a tool for distal tephrostratigraphy. Journal of Volcanology and Geothermal Research 177: 1-18.

Sevink J, van Bergen MJ, van der Plicht et al. 2011. Robust date for the Bronze Age Avellino eruption (Somma-Vesuvius): 3945 ± 10 cal BP (1995 ± 10 cal BC). Quaternary Science Reviews 30: 1035–1046.

Siani G, Paterne M, Arnold M et al. 2000. Radiocarbon Reservoir Ages in the Mediterranean Sea and Black Sea. Radiocarbon 42: 271–280.

Siani G, Sulpizio R, Paterne M et al. 2004. Tephrostratigraphy study for the last 18,00014C years in a deep-sea sediment sequence for the South Adriatic. Quaternary Science Reviews 23: 2485–2500.

Smith VC, Isaia R, Pearce NJG 2011. Tephrostratigraphy and glass compositions of post-15 kyr Campi Flegrei eruptions: Implications for eruption history and chronostratigraphic markers. Quaternary Science Reviews 30: 3638–3660.

Wulf S, Kraml M, Brauer A et al. 2004. Tephrochronology of the 100ka lacustrine sediment record of Lago Grande di Monticchio (southern Italy). Quaternary International 122: 7–30.

Wulf S, Kraml M, Keller J 2008. Towards a detailed distal tephrostratigraphy in the central Mediterranean: the last 20,000 yrs record of Lago Grande di Monticchio. Journal of Volcanology and Geothermal Research 177: 118-132.

Zanchetta G, Sulpizio R, Roberts CN et al. 2011. Tephrostratigraphy, chronology and climatic events of the Mediterranean basin during the Holocene: an overview. The Holocene 21 (1): 33-52.